

University of Montana

## ScholarWorks at University of Montana

---

Graduate Student Theses, Dissertations, &  
Professional Papers

Graduate School

---

1987

### A comparison of the thermal profiles of two adjacent thrust plates in western Montana

Christopher Paul Weiss  
*The University of Montana*

Follow this and additional works at: <https://scholarworks.umt.edu/etd>

**Let us know how access to this document benefits you.**

---

#### Recommended Citation

Weiss, Christopher Paul, "A comparison of the thermal profiles of two adjacent thrust plates in western Montana" (1987). *Graduate Student Theses, Dissertations, & Professional Papers*. 7525.  
<https://scholarworks.umt.edu/etd/7525>

This Thesis is brought to you for free and open access by the Graduate School at ScholarWorks at University of Montana. It has been accepted for inclusion in Graduate Student Theses, Dissertations, & Professional Papers by an authorized administrator of ScholarWorks at University of Montana. For more information, please contact [scholarworks@mso.umt.edu](mailto:scholarworks@mso.umt.edu).

COPYRIGHT ACT OF 1976

THIS IS AN UNPUBLISHED MANUSCRIPT IN WHICH COPYRIGHT  
SUBSISTS. ANY FURTHER REPRINTING OF ITS CONTENTS MUST BE  
APPROVED BY THE AUTHOR.

MANSFIELD LIBRARY  
UNIVERSITY OF MONTANA  
DATE: 1987



A COMPARISON OF THE THERMAL PROFILES OF TWO  
ADJACENT THRUST PLATES IN WESTERN MONTANA

By

Christopher Paul Weiss

B.S., University of Michigan, 1985

Presented in partial fulfillment of the requirements

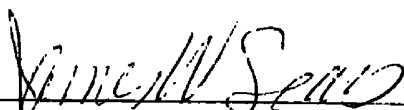
for the degree of

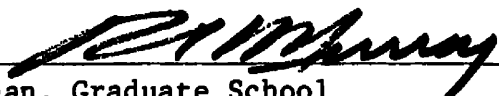
Master of Science

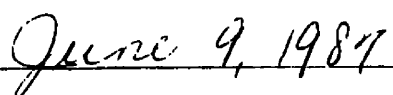
University of Montana

1987

Approved by

  
Chairman, Board of Examiners

  
Dean, Graduate School

  
Date

UMI Number: EP38326

All rights reserved

**INFORMATION TO ALL USERS**

The quality of this reproduction is dependent upon the quality of the copy submitted.

In the unlikely event that the author did not send a complete manuscript and there are missing pages, these will be noted. Also, if material had to be removed, a note will indicate the deletion.



UMI EP38326

Published by ProQuest LLC (2013). Copyright in the Dissertation held by the Author.

Microform Edition © ProQuest LLC.

All rights reserved. This work is protected against unauthorized copying under Title 17, United States Code



ProQuest LLC.  
789 East Eisenhower Parkway  
P.O. Box 1346  
Ann Arbor, MI 48106 - 1346

Weiss, Christopher P., M.S., June, 1987

Geology

A Comparison of the Thermal Profiles of Two Adjacent Thrust Plates  
in Western Montana (76 pp.)

Director: James W. Sears



Two major thrust plates overlap in a broad structural zone in western Montana. During the late Cretaceous the western (hangingwall) plate, cored by the present-day Idaho batholith, thrust over the eastern (footwall) plate. As a result, the eastern plate underwent deformation and metamorphism, now evident as a southwest-dipping fabric in rocks exposed in a corridor extending 75 km northwest and southeast of Missoula, Montana.

Continental accretion and the early stages of Idaho batholith intrusion thickened the proto-western plate during 105-85 Ma. Heat from the early stages of batholith emplacement metamorphosed Proterozoic Belt Supergroup rocks of the northern border zone to upper amphibolite grade. From 85-82 Ma, the thickened western plate failed and thrust over the eastern plate, as evidenced by rapid uplift and cooling in rocks of the western plate. Decreasing overburden, due to thrusting in the hangingwall plate, enabled lower pressure and temperature mineral assemblages to overprint the older assemblages. A fabric associated with the thrusting gradually migrated into footwall rocks to become a regional, southwest-dipping fabric.

Temperature increase from the overlying western plate formed new minerals in the regional fabric within Proterozoic Belt Supergroup rocks of the eastern plate, overprinting Precambrian burial metamorphic assemblages. At the highest level, the cleavage crosscut the late Cretaceous Golden Spike Formation, a syntectonic conglomerate derived from the western plate. Regional fabric formation, contemporaneous with the emplacement of the Garnet stock at 82 Ma defined a southeast plunging fold system. At deeper levels, rocks formed broad folds, and pelitic formations deformed by simple shear, with temperatures sufficient to grow biotite and chlorite. Shallow level rocks formed tighter folds, thrust, and underwent ductile deformation locally near thrusts. Temperatures in the southeast portion of the footwall were higher than those at correlative levels in the northwest; late Cretaceous intrusives in the southeast indicate that this was an area of higher heat flow.

TABLE OF CONTENTS

	page
Abstract.....	ii
Table of Contents.....	iii
List of Figures.....	iv
Acknowledgements.....	vi
Thermal Effects of Thrust Faulting.....	1
Geologic Setting.....	7
Metamorphism and Thermal Profiles.....	11
Western Plate.....	11
Eastern Plate.....	16
Deformation Style and Timing of Late Cretaceous Events .....	30
Western Plate.....	30
Eastern Plate-Deformation Style.....	33
Eastern Plate-Timing of Late Cretaceous Events.....	44
Geologic History.....	49
Summary.....	54
References.....	58
Appendix A, Stratigraphy and Structural Behavior of Units.....	64
Appendix B, Western Plate Mineral Assemblages.....	67
Appendix C, Eastern Plate Mineral Assemblages.....	68
Appendix D, Strain Measurements.....	72

LIST OF FIGURES

Figure	page
1. Diagram of initial conditions after thrusting from a thermal model for overthrusting.....	3
2. Diagram of pressure-temperature-time paths for overthrustured regions with different uplift histories.....	4
3. Regional setting of the western and eastern plates.....	8
4. Photomicrograph of cleavage refraction in the lower Prichard Formation.....	10
5. Photomicrograph of spaced cleavage in the Cretaceous Blackleaf Formation.....	10
6. Chart of timing constraints for late Cretaceous deformation in the western and eastern plates.....	12
7. Pressure-temperature diagram of reported mineral assemblages from the western plate's M1 and M2 metamorphic events.....	13
8. Pressure-time chart showing the changes in pressure conditions in the western plate in the late Cretaceous.....	14
9. Map of Precambrian burial metamorphism within the overthrustured zone of the eastern plate.....	18
10. Photomicrograph of biotite from Precambrian burial metamorphism in the lower Prichard Formation.....	20
11. Photomicrograph of chloritized and sheared Precambrian biotite aligned with the Cretaceous fabric in the lower Prichard Formation.....	20
12. Map of Cretaceous metamorphism within the overthrustured zone of the eastern plate.....	21
13. Photomicrograph of biotite aligned with the Cretaceous fabric in the lower Prichard Formation.....	23
14. Schematic down plunge projection of the overthrustured zone of the eastern plate, showing temperature data and brittle/ductile behavior of faults.....	27

15.	Location map for key timing indicators of the late Cretaceous deformation.....	31
16.	Schematic section through the overthrust zone showing relation between fabrics and metamorphic events in the western and eastern plates.....	33
17.	Photomicrograph of pyrites with pressure shadows from the upper Prichard Formation.....	35
18.	Photomicrograph showing close-up view of Figure 17.....	35
19.	Photomicrograph of a deformed sandstone dike and pyrite pressure shadows from the upper Prichard Formation....	37
20.	Sketch map and projection to a thin section sketch showing the relation of outcrop data to microscopic deformation features of the eastern plate.....	38
21.	Strain facies map showing the relative strain intensity within the overthrust area of the eastern plate.....	40
22.	Map of pi diagrams of cleavage and lineations for the overthrust zone of the eastern plate.....	45
23.	Pressure-temperature diagram with thermal profiles from the western and eastern plates.....	50

## ACKNOWLEDGEMENTS

To Dr. Jim Sears, my advisor, instructor, and friend, I express my most sincere gratitude. His suggestions, good humor, and ability to see the "big picture" were priceless. Dr. Steve Sheriff made valuable suggestions during the editing of the thesis. Dr. Jack Donahue helped edit the thesis and, along with Lydia Donahue, gave me an adopted home in Missoula. To Dr. Don Winston, who introduced me to the Belt Basin and some great music, I express my thanks. His wisdom and wit are very special.

Support for the research came from the McDonough Research Fund and a grant from Sigma Xi, the Scientific Research Society.

Several others provided support during my pursuits in geology. Dr. Bruce Wilkinson, at the University of Michigan, introduced me to research, writing, carbonate petrology, and structural geology ("rocks bend, rocks break"). At the University of Montana, the faculty and my fellow graduate students, especially Rob Thomas and Anneliese Ripley, supplemented my coursework with stimulating conversations and taught me how to think. My parents, Francis and Betty Weiss, family, and lifelong friend, David Diller, provided me with moral support. I dedicate this thesis to my father, Francis Weiss, a man I greatly admire.

## THERMAL EFFECTS OF THRUST EMPLACEMENT

The study of thermal profiles in exposed thrust sheets may lead to a better understanding of the history of an orogenic belt. The preserved pressure and temperature paths of the rocks can untangle the often complex web of thermal and mechanical processes responsible for the evolution of an orogenic belt. Many factors affect these processes and most authors (e.g. Oxburgh and Turcotte, 1974, Brewer, 1981, and England and Thompson, 1984) include these factors in models they develop for the thrusting process. After the emplacement of the thrust, models predict the changes in temperature of the allochthonous and autochthonous rocks. Various methods enable one to determine the maximum temperatures preserved in the rocks. Whenever possible, authors (e.g. Crawford and Mark, 1982, and Thompson and England, 1984) use the maximum temperature data and the pressure-temperature-time (PTt) paths of specific horizons within the sheet to reconstruct the paleogeothermal gradient at the time of overthrusting.

Large overthrusts cause major perturbations in the regional geothermal gradient, since the additional overburden causes temperatures and pressures to change. Many factors effect these changes in allochthonous and autochthonous rocks. The key factors include the total radiogenic heat supply of the rocks, the mantle heat supply, the thermal conductivities of various lithologies (England and Thompson, 1984, and Davy and Gillit, 1986), the initial surface heat

flow and heat production, and the geothermal gradient of the crust and its change with time (Cook, 1983, and Royden and Hodges, 1984). In addition, other physical parameters are important, such as the thickness of the thrust sheet and the rate of erosion and uplift (Oxburgh and Turcotte, 1974, and England and Thompson, 1984). If more than one thrust was involved, one must consider the number of thrusts and the time between successive thrusts (Davy and Gillit, 1986). Thermal models must include all of the above thermal and mechanical factors to duplicate actual conditions during thrusting.

Thermal models for areas of overthrusting are necessarily complicated. Still, most models include similar geologic assumptions and suggest similar conclusions. For example, many models (Oxburgh and Turcotte, 1974, Brewer, 1981, Cook, 1983, and England and Thompson, 1984) treat thrusting as a geologically rapid event and therefore believe erosion has a significant effect only after the emplacement of a thrust. In their study of the Eastern Alps, Oxburgh and Turcotte (1974) used a value of 3 cm/yr for the speed of thrust faulting based on the assumption that regional thrusting should relate to plate tectonics and should have a similar rate of movement. Immediately after the emplacement of the thrust plate, the thermal profile has a sawtooth shape (Figure 1), assuming that the overthrust and underlying blocks retain their approximate original thermal profile (Oxburgh and Turcotte, 1974). This assumption would be invalid if the blocks underwent significant thermal equilibration during thrusting. However, assuming rapid rates of thrusting, Oxburgh and Turcotte (1974)

suggested that thermal equilibration during thrusting is low enough to make the sawtooth shaped thermal profile useful as a first approximation for conditions immediately after thrusting. After thrust emplacement, pressure increases dramatically, since the tectonically thickened pile has not yet begun to erode (Richardson and England, 1979). These conditions during and immediately after the thrust greatly influence the pressure and temperature paths later followed by the rocks.

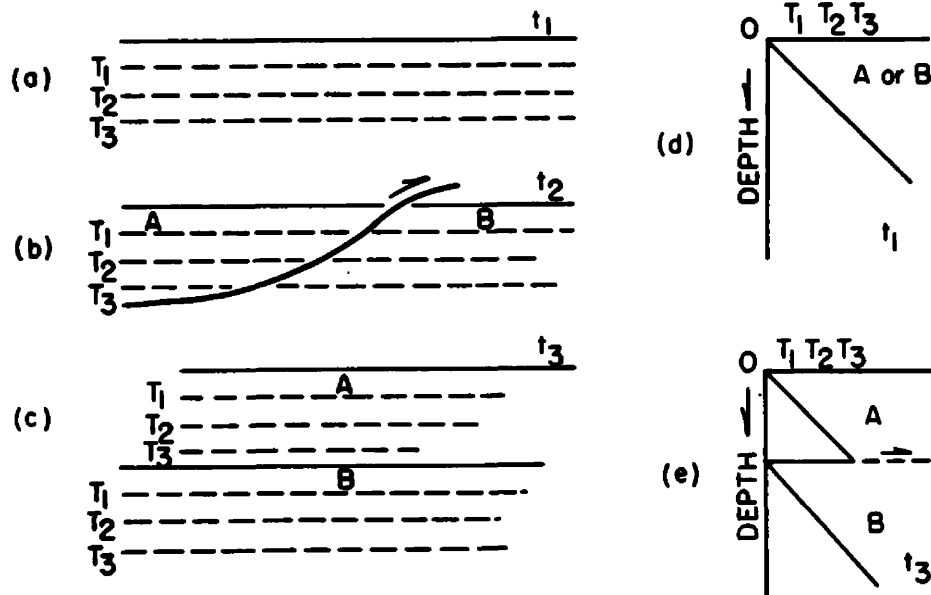


Figure 1. Thrusting model, which assumes thrusting is an instantaneous event: (a) crustal profile of presumed initial ( $t_1$ ) condition;  $T$ =temperature with  $T_1 < T_2 < T_3$  and associated thermal gradient shown in (d); (b) incipient thrust; (c) situation immediately after thrusting, giving rise to thermal profile (e). (from Oxburgh and Turcotte, 1974)

After thrusting occurs, models predict the changes of temperature and pressure as the rocks uplift, erode, and equilibrate with the new thermal conditions. For a few million years temperatures remain low in the footwall blocks with thrust plates up to 25 km thick because of low thermal conductivity (0.003-0.009 cal/sec °C) (Oxburgh and Turcotte, 1974), but gradually, the thermal profiles of the blocks equilibrate with the new conditions. The temperatures in the pile rise until the onset of uplift and erosion (Oxburgh and Turcotte, 1974), but the maximum temperature often occurs after the start of erosion (England and Richardson, 1977). According to England and Thompson (1984), with geologically conservative erosion rates of 0.1-1.7 mm/yr, rocks do not reach their maximum temperature until they complete 20-40 % of their final total uplift and erosion (Figure 2). In general, a rock's

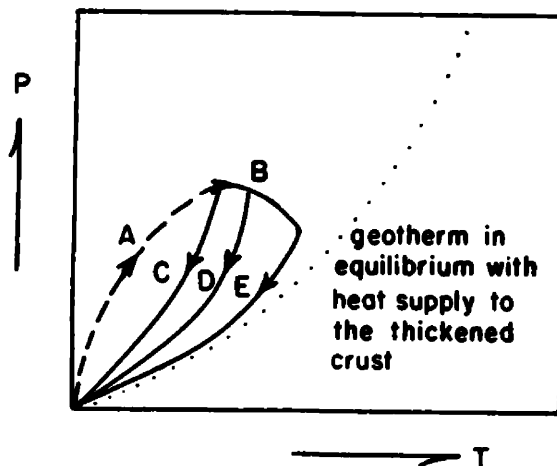


Figure 2. Schematic pressure-temperature-time paths of rocks undergoing rapid burial on path A, followed by uplift histories that are progressively longer from path C to path D to path E. Point B represents a phase of heating with little erosion. (from England and Thompson, 1984)

temperature increases for a longer period of time when it is buried deeper in the thrust blocks (England and Richardson, 1977, and Royden and Hodges, 1984). Most horizons in a tectonically thickened pile lie within 50° C of the maximum temperature for at least one third of their total burial and uplift time (England and Thompson, 1984). Erosion often interrupts heating of the pile, since it brings the constant cold temperature of the surface closer to any given stratigraphic horizon, thus reducing that horizon's final equilibrium temperature (Oxburgh and Turcotte, 1974, and Angevine and Turcotte, 1983).

These processes, uplift and erosion, often expose profiles across all or part of the thrust sheet and those rocks underlying the thrust. These exposed thrust terrains may allow study of the geothermal gradient preserved during the heating event. By using the metamorphic mineral assemblages exposed at the surface after the event, geologists can infer the geothermal profile during metamorphism (Thompson and England, 1984). Metamorphic mineral assemblages establish this profile by providing isograds (lines of equal temperature) based on the equilibration temperatures of different metamorphic minerals (Crawford and Mark, 1982). Illite crystallinity, vitrinite reflectance, pyrolysis, thermal alteration index data, and conodont alteration index data also establish isograds in regions of low-grade metamorphism. In low-grade metamorphic thrust sheets of the Idaho-Utah-Wyoming thrust belt, Mitra and Yonkee (1984) used illite crystallinity to establish temperatures of cleavage formation. Bostick (1974) used thermal alteration index data as a guide to grades of

metamorphism, while Harris (1981) correlated the color of conodonts with temperatures of low-grade metamorphism. Finally, Hood and et al. (1975) correlated the above thermal maturation indicators, as well as vitrinite reflectance and pyrolysis, with a level of organic maturation (LOM) scale, which enables one to find the maximum temperature achieved by sediments. The array of maximum temperatures from prograde metamorphism at different horizons within the pile, found with methods outlined above, establishes a maximum thermal profile for a thrusting plate.

This array of temperatures cannot, however, determine the paleogeothermal gradient at any one time during the thrusting and heating process (England and Richardson, 1977). According to Thompson and England (1984), additional data is required to constrain the paleogeothermal gradient. They suggested using zoned garnets and other porphyroblasts as portions of the PTt path for that horizon. Geochronology and inclusion data also isolate portions of the PTt path (Royden and Hodges, 1984). Unfortunately, data from techniques that isolate portions of the PTt path is often unavailable in areas of low-grade metamorphism. In these areas, the various temperature points are used as a rough guide to the paleogeothermal gradient or, in conjunction with heat-flow modeling techniques, as a constraint for PTt paths (Angevine and Turcotte, 1983). Even without precise PTt path data, a profile of maximum temperatures, together with data on the timing and style of deformation, yields much information about the thermal history of an overthrust region.

This study looks at one such area of overthrusting in western Montana (figure 3), where uplift and subsequent erosion exposed both the hangingwall and footwall plates. The thermal profiles of these plates and much other information enabled me to reconstruct the area's tectonic history. To establish the maximum thermal profile of the exposed footwall plate, I used a combination of metamorphic mineral assemblages and indicators of low grade metamorphism. Metamorphic mineral assemblages from the adjacent hangingwall plate, reported in the literature by several workers (e.g. Chase, 1973, Childs, 1982, and Hietanen, 1984) allowed me to determine its thermal profile and compare it with that of the footwall.

#### GEOLOGIC SETTING

Two major thrust plates overlap in a broad structural zone near Missoula, Montana (Figure 3). The western plate forms the hangingwall and the eastern plate forms the footwall. These plates are distinct structural blocks with no large-scale thrusts within each plate (Figure 3). Granitic rock of the Idaho batholith cores the western plate, surrounded by a wide border zone of regionally metamorphosed middle Proterozoic Belt Supergroup rocks, decreasing in grade away from the granite (Hyndman et al., 1987). The eastern plate consists of a complete section of middle Proterozoic Belt Supergroup rocks, reportedly up to 20 km thick (Harrison, 1972). Overlying the Belt Supergroup rocks are Paleozoic rocks (primarily limestones) and

Mesozoic rocks (primarily sandstones, shales, and volcanics) approximately 10 km thick (Ruppel et al., 1981). Details of the stratigraphy and thicknesses of units in the eastern plate are found in Appendix A. The eastern plate does not contain pressure sensitive metamorphic minerals that would have enabled me to measure pressure directly, but the reported stratigraphic thicknesses in the eastern plate and structural projections allowed me to estimate minimum pressures experienced at different levels during thrusting and metamorphism.

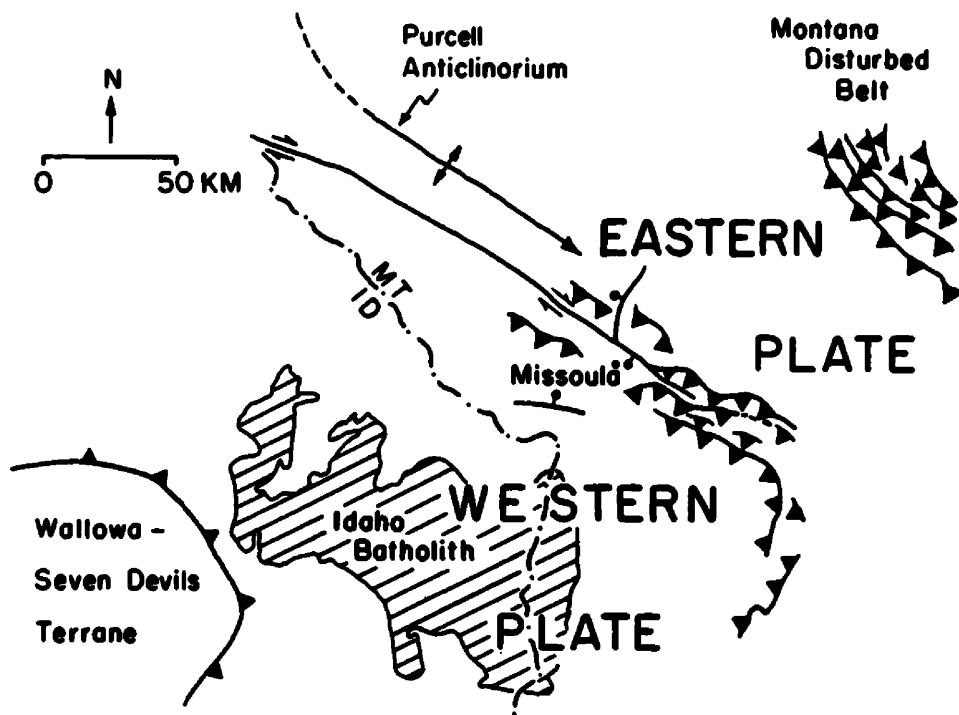


Figure 3. Regional setting of the western and eastern plates.

The deformation and metamorphism of rocks in the eastern plate occurred during the late Cretaceous, when rocks in the western plate thrust about 50 km to the northeast over the eastern plate (Sears, 1986). A series of thrust faults defines the present-day northeast margin of the western plate (Figure 3). In general, these thrusts placed unclesaved Proterozoic Belt Supergroup rocks over Paleozoic and Mesozoic rocks of the eastern plate. Within a 150 km length of the overlap zone, subsequently exposed by erosion, a single cleavage fabric cuts eastern plate rocks up to late Cretaceous in age (Figures 4 and 5). Folds and minor structures within the zone define a regional plunge to the southeast (Sears and Weiss, 1986). The relatively simple, continuous nature of the structures within the overlap zone enabled me to closely tie events associated with the footwall deformation to events in the hangingwall.

The purpose of this study was to determine the thermal profiles of the two plates and use them to constrain reconstructions of the tectonic history. Metamorphic phases in the two plates and associated variations in temperature and pressure enabled me to estimate the maximum thermal conditions achieved within the plates. I then use the profiles, together with information on the deformation and timing, to describe the middle to late Cretaceous tectonic history for the region.



Figure 4. Photomicrograph of cleavage and refraction of cleavage in the Proterozoic lower Prichard Formation (sample 127). Field of view is 3.5 mm.

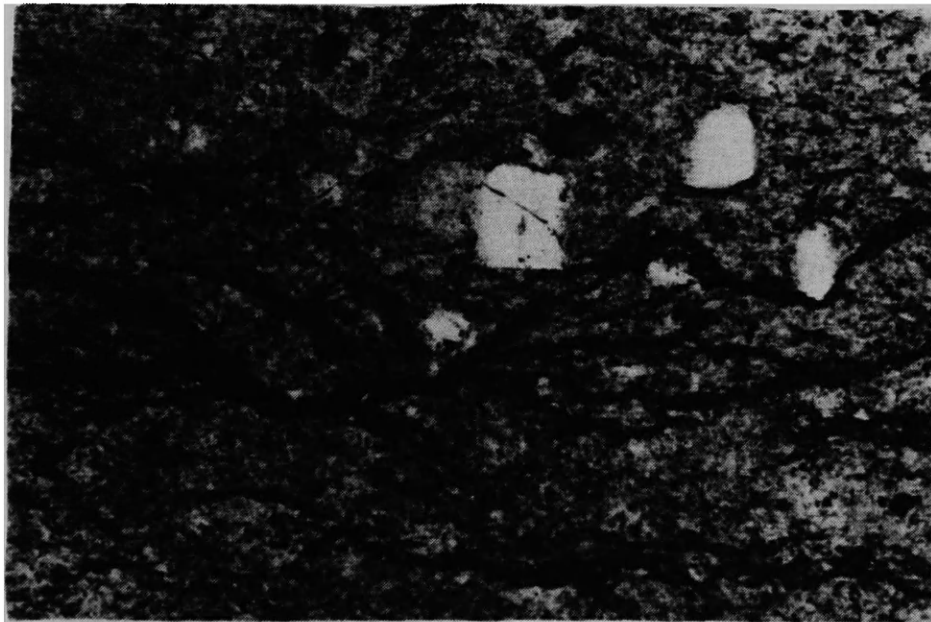


Figure 5. Photomicrograph of spaced cleavage in the Cretaceous Blackleaf Formation (sample 3). Field of view is 3.5 mm.

## METAMORPHISM AND THERMAL PROFILES

### Western plate

The accretion of the Wallowa-Seven Devils terrane in north-central Idaho along a continental suture west of the present-day Idaho batholith (Figure 3), the emplacement of the Idaho batholith and related plutons, and regional uplift of the terranes and Idaho batholith region, gave rise to two thermal events in the western plate (Hyndman et al., 1987). The first thermal event, M1, occurred during the early stages of emplacement of the Idaho batholith and resulted in metamorphic mineral assemblages of the Barrovian facies series (Hietanen, 1984) in Belt Supergroup rocks near the batholith. Subsequent regional uplift during the second thermal event, M2, resulted in lower pressure and temperature mineral assemblages, which overprinted M1 assemblages. The accretion affected both thermal events and their associated mineral assemblages.

Accretion of the Wallowa-Seven Devils terrane (Figure 3) began about 105 Ma, with thrust faulting and mesoscopic deformation within the terrane until 95 Ma (Lund and Snee, 1985). By 95-85 Ma deformation had shifted to the suture zone between the terrane and the present-day Idaho batholith border zone, but between 87-75 Ma pluton emplacement closed the suture zone (Criss and Fleck, 1987) (Figure 6). Most of the

Figure 6. Timing chart for late Cretaceous events in the western and eastern plates.



northern portion of the Idaho batholith formed after deformation began in the suture (Criss and Fleck, 1987). Toth (1987) reported that early tonalites and quartz diorites of the northern Idaho batholith intruded between 100-80 Ma, while Lund and Snee (1985) reported that early tonalites intruded between 95-85 Ma (Figure 6), associated with the first thermal event, M1. The M1 metamorphism was contemporaneous with the emplacement of early quartz diorite and tonalite (Toth, 1987). Appendix B lists M1 mineral assemblages reported by many workers from metamorphosed Belt Supergroup rocks of the northern border zone. Most of the assemblages plot in the upper amphibolite facies (Figure 7).

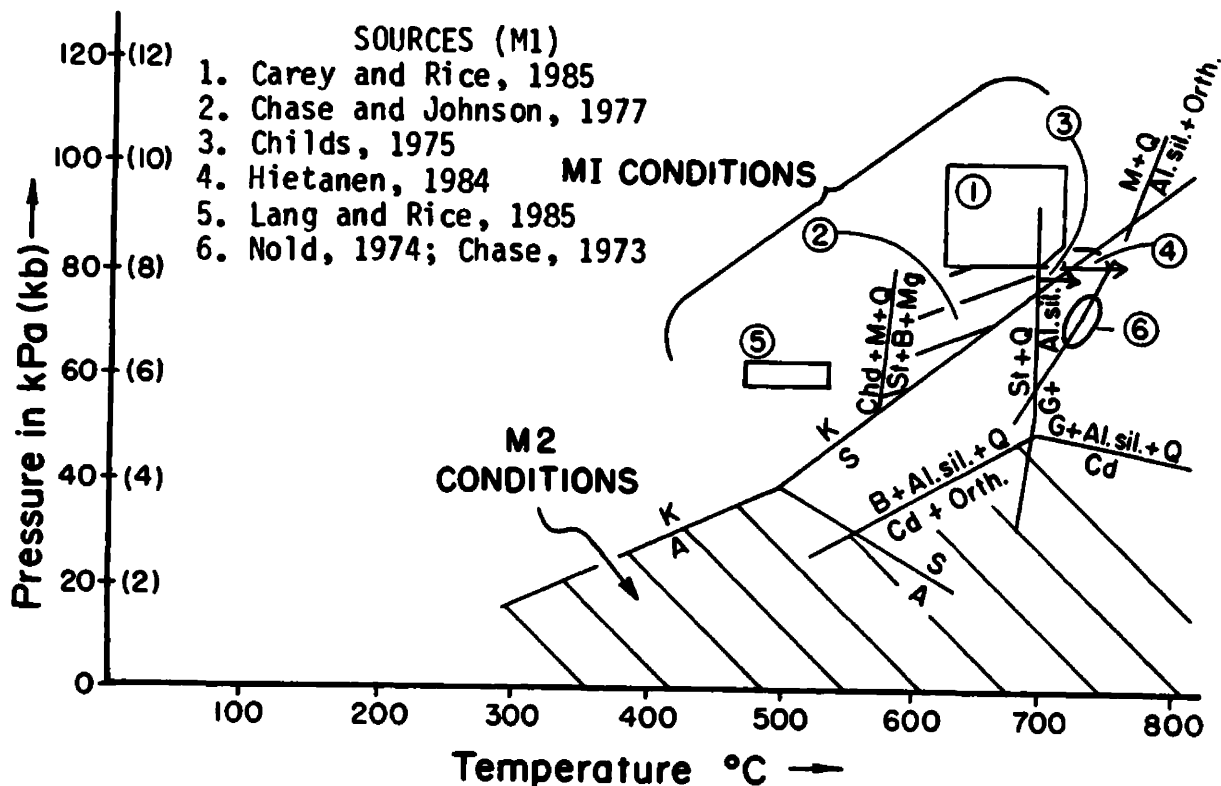


Figure 7. Pressure-temperature diagram illustrating reported assemblages and conditions for the M1 and M2 metamorphic events in the western plate.

The maximum temperatures and pressures of M1 range between 550–700°C and 55–80 kPa (5.5–8.0 kb), respectively. The assemblage sillimanite-biotite-muscovite-orthoclase-quartz (Chase, 1973 and Nold, 1974) defines these values, since the rocks entered the sillimanite-orthoclase zone along a path through the staurolite and kyanite zones (Hietanen, 1984). Schematically, these pressures represent values recorded in the western plate during the approximate period of M1 metamorphism, 95–85 Ma (Figures 8).

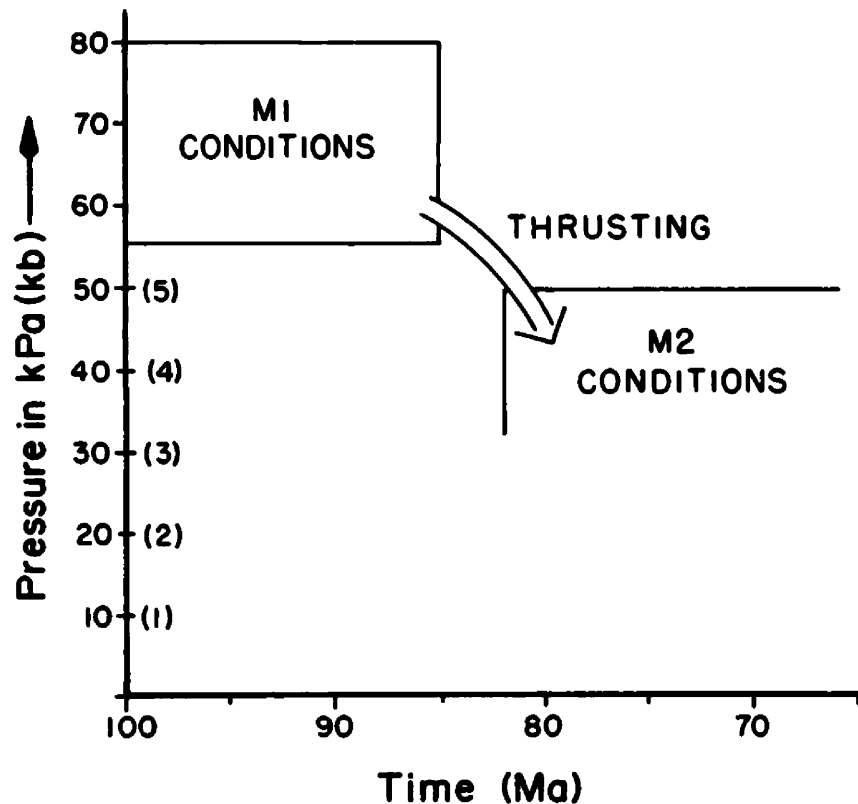


Figure 8. Pressure-time chart, indicating the pressure conditions in the western plate during the M1 and M2 metamorphic events and the change, due to thrusting or gravitational spreading to the northeast.

From about 85-75 Ma (Figure 6) (Lund and Snee, 1985), rapid uplift of the batholith region established conditions of lower pressure for minerals that crystallized during the M2 event (reported assemblages in Appendix B). Lund and Snee (1985) concluded that plutons emplaced at 15 km in terranes near the suture zone underwent rapid uplift from 85-75 Ma, since they cooled very quickly during emplacement. In plutonic rocks emplaced in the suture zone, Criss and Fleck (1987) found that potassium-argon ages of biotite and hornblende were very close, also representing rapid cooling. From the blocking temperatures of biotite and hornblende, 280°C and 500°C, respectively (Cliff, 1985), I estimated cooling rates from 34-314°C/million years (from Criss and Fleck's (1987) reported data). These rates vary from very rapid (England and Thompson, 1984) to almost instantaneous cooling. To cool 220°C almost instantaneously in suture zone plutons emplaced at depths greater than 10-15 km (Criss and Fleck, 1987) is impossible with geologically conservative erosion rates of 0.1 to 1.7 mm/yr (England and Thompson, 1984); higher erosion rates or tectonic processes are required. With an average geothermal gradient of 30°C/km in the uppermost crust (Oxburgh and Turcotte, 1974), the loss of overburden by thrusting, gravitational spreading, or very rapid uplift and erosion, of at least 7 km of rock would enable the plutons to quickly reequilibrate at temperatures near the blocking temperature of biotite. Pressure conditions from minerals formed further east during M2 metamorphic conditions, also suggest a loss of at least 7 km of overburden. These M2 minerals that formed after the rapid uplift and

unroofing, such as andalusite and cordierite (Figure 7), recorded pressures of up to 50 kPa (5 kb). As with the M1 values, I plotted the pressures for the approximate duration of the M2 metamorphism (Figure 8).

After the M1 metamorphism, the pressure change to M2 conditions resulted in lower pressure, M2 metamorphic mineral assemblages superimposed on M1 metamorphic assemblages in rocks at given sites in the deepest levels of the western plate now exposed. I believe that thrusting to the northeast, over the eastern plate, was the mechanism for the decrease in pressure conditions. Though I will describe the thrusting in greater detail below, one should note that thrusting took place after the M1 event, but apparently before the M2 event, giving rise to the metamorphic event in the eastern plate.

### Eastern plate

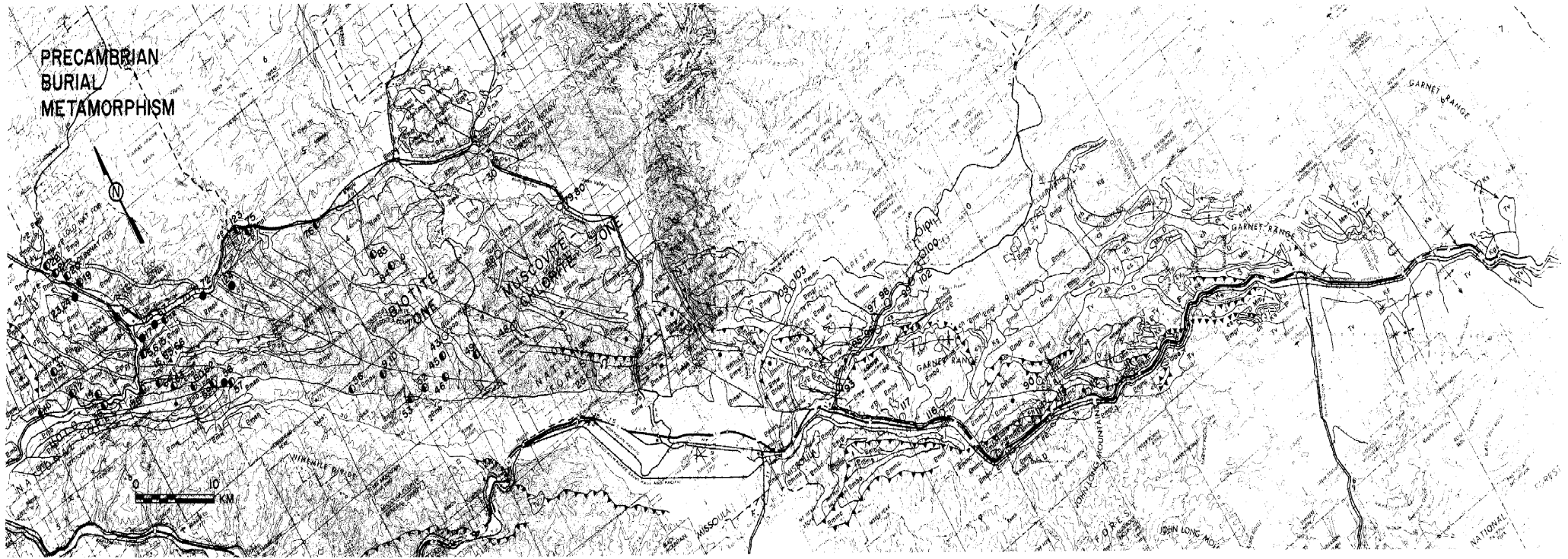
The metamorphism preserved in the footwall plate overprints an older fabric from Precambrian burial metamorphism (Norwick, 1972). There is no other pre-existing fabric in this part of the eastern plate. The Precambrian metamorphism reached the garnet-biotite zone, while the Cretaceous overprint only reached the biotite zone. Due to the similar mineralogies of the two metamorphic assemblages, I found it necessary to analyze the minerals formed during each phase separately, to clearly define the Cretaceous isograds and maximum thermal profile.

Within the exposed eastern plate, the highest grade Precambrian burial assemblages (Appendix C) formed in the lowest units of the Belt

Supergroup. At the base of the Belt Supergroup, the Prichard Formation contained consistent assemblages of biotite-muscovite-quartz +/- plagioclase, with isolated occurrences of garnet (Figure 9). Contrary to previous work (Norwick, 1972), I found biotite from Precambrian burial metamorphism throughout all of the Ravalli Group, as well as the Prichard Formation, with the exception of quartzites in the Revett Formation. Units stratigraphically above the Ravalli Group contained assemblages of plagioclase-muscovite, +/-chlorite. The Precambrian biotite within the Ravalli Group and Prichard Formation differed from that formed in the Cretaceous in that the Precambrian burial metamorphic biotite grew in rounded aggregates of random orientation (Figure 10), though these were sometimes sheared and chloritized in zones of high strain during the Cretaceous metamorphism (Figure 11).

The highest temperatures and pressures preserved from the Cretaceous metamorphism in exposed rocks also formed in the Prichard Formation (Figure 12). Unlike assemblages from the Precambrian burial metamorphism, however, the highest grade assemblage (Appendix C), biotite-chlorite-muscovite-quartz, +/-plagioclase, formed only in the lowermost Prichard Formation. From a minimum stratigraphic depth of 15 km, without taking into account Mesozoic sediments or the overlying hangingwall plate, the above assemblage represents a temperature at 50 kPa (5 kb) of at least 450°C (Winkler, 1982). According to Winkler (1982), the assemblage biotite-chlorite-quartz is stable between 450 to 525°C at 50 kPa (5 kb). The Cretaceous biotite probably did not simply recrystallize from the Precambrian biotite at an appropriate

Figure 9. Map of Precambrian burial metamorphism showing sample locations and the line between the Precambrian metamorphic biotite and chlorite-muscovite zones in this study area. Blackened circles indicate a sample with Precambrian biotite and garnet, half-blackened circles indicate samples with biotite only, and empty circles indicate samples with no biotite or garnet. See Appendix C for exact Precambrian burial assemblages.



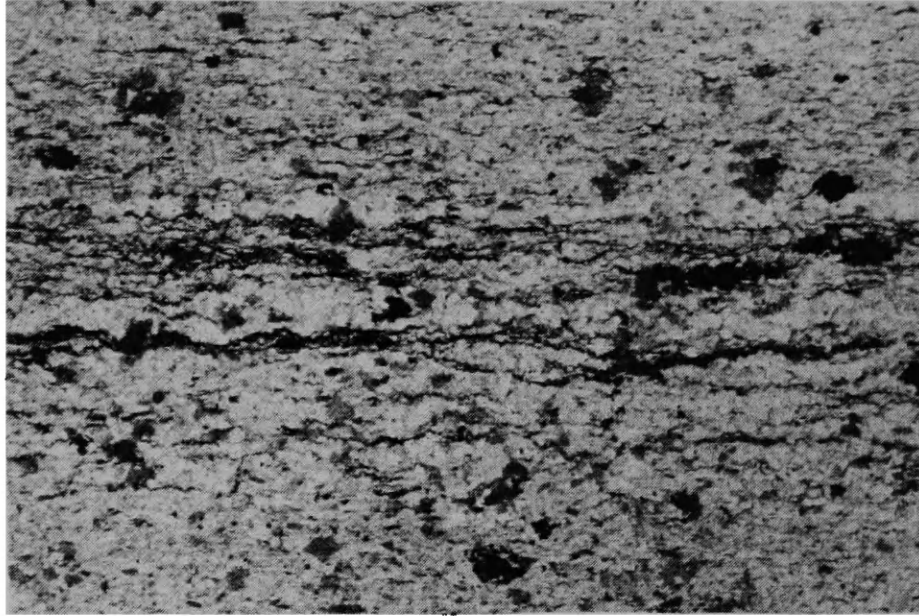


Figure 10. Photomicrograph of randomly-oriented biotite from Precambrian burial metamorphism (lower Prichard Formation, sample 14). Field of view is 3.5 mm.

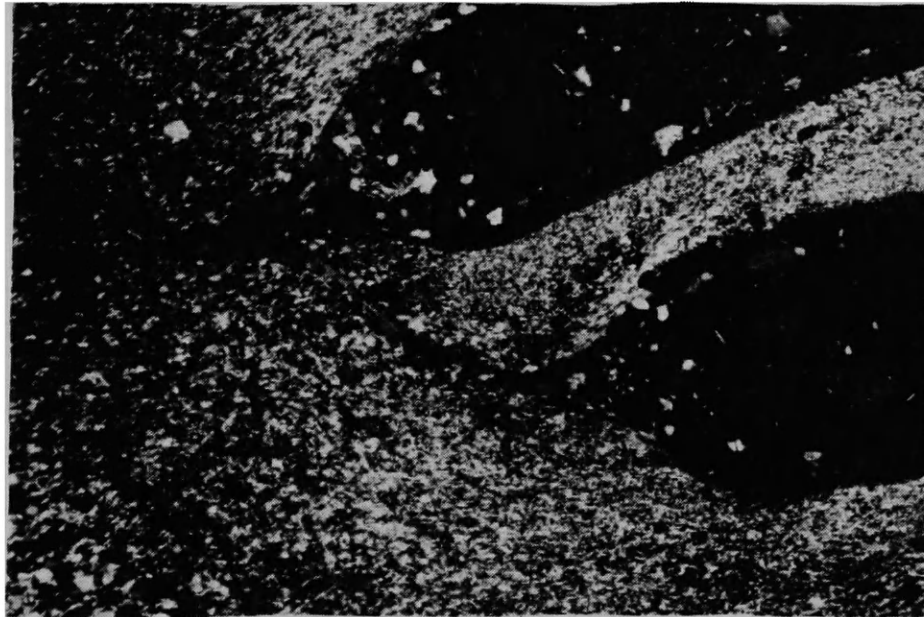


Figure 11. Photomicrograph illustrating sheared and chloritized Precambrian burial metamorphic biotite now aligned with the regional late Cretaceous fabric. Field of view is 3.5 mm.

**Figure 12. Map of Cretaceous metamorphism showing sample locations  
Half-blackened circles indicate sample with Cretaceous  
biotite. All samples contained minerals aligned with the  
regional fabric (Appendix C, Cretaceous assemblages).**



temperature, since the Cretaceous metamorphism chloritized most of the Precambrian biotite prior to the growth of the new biotite (Figure 11). I distinguished Cretaceous biotite in thin-section by its elongate crystals and growth in the regional Cretaceous fabric, at some angle to bedding (Figure 13). While the biotite isograd represents the highest grade of Cretaceous metamorphism exposed in the eastern plate, other mineral assemblages recorded lower temperature conditions at stratigraphically higher levels.

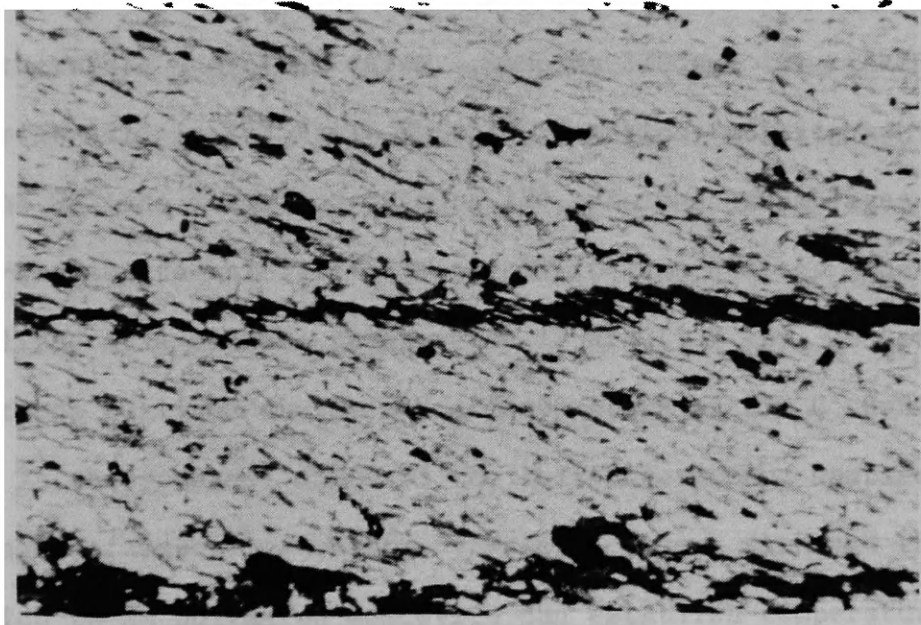


Figure 13. Photomicrograph of biotite aligned with the late Cretaceous fabric at approximately 30 degrees to bedding (horizontal), from the lower Prichard Formation, sample 8. Field of view is 3.5 mm.

In rocks of the Ravalli Group, the Cretaceous metamorphism chloritized Precambrian biotites, and in the Ravalli Group and

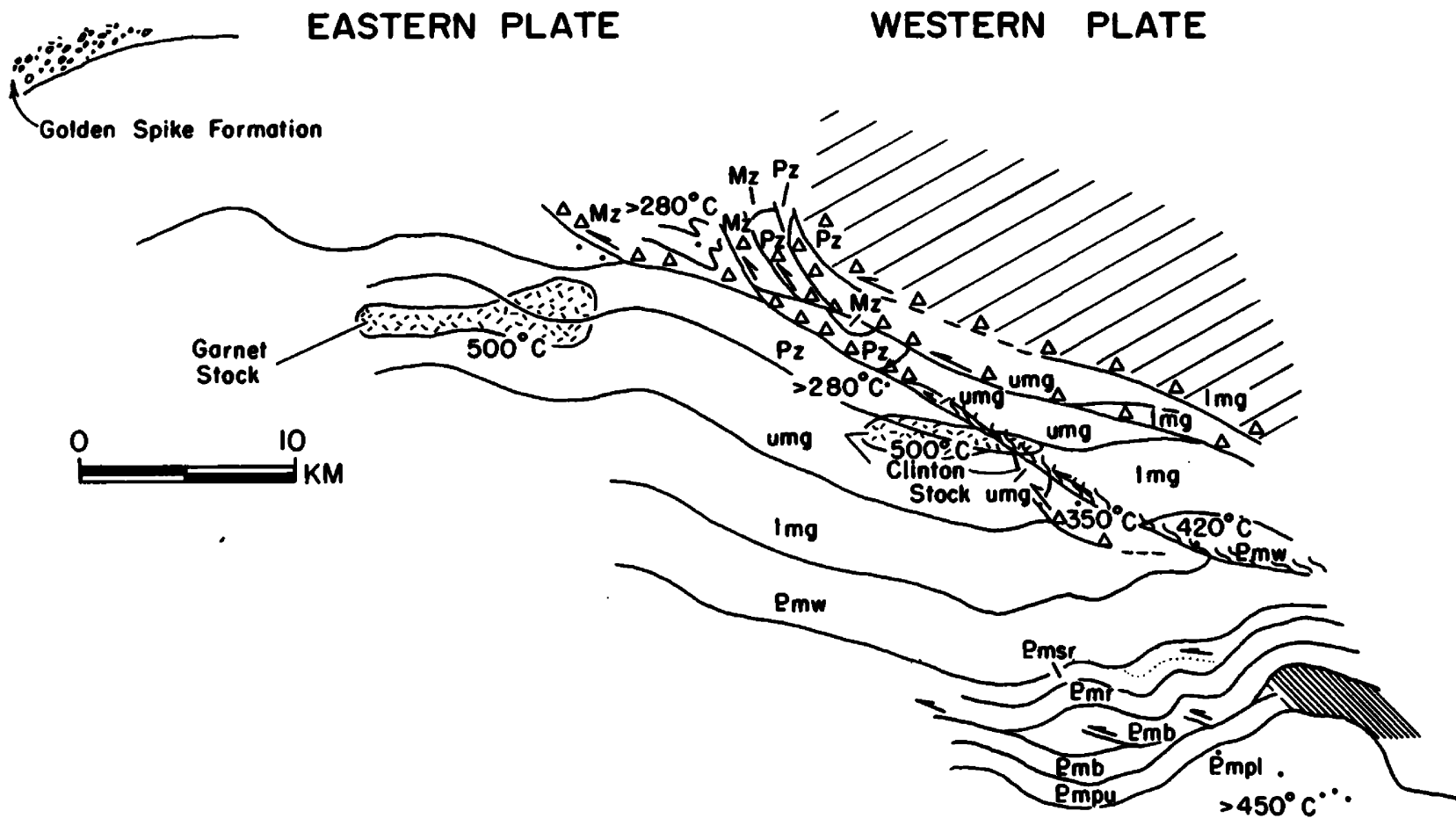
stratigraphically higher levels, chlorite crystallized as elongate fibers aligned with the regional fabric. In sample 128, from just north of Missoula, Montana (Figure 12), in the stratigraphically higher Wallace Formation, coexisting minerals included talc, calcite, dolomite, muscovite, and quartz. With an estimated stratigraphic depth including only the overlying Belt Supergroup Formations and Paleozoic rocks, at a pressure of 25 kPa (2.5 kb), the sample reached a temperature of at least 420°C (Hyndman, 1985). However, this value assumes a low partial pressure of carbon dioxide (0.25), probably not a valid assumption for the calc-silicate system in the Wallace Formation, and is therefore a minimum value. Samples 130 and 131, taken from a Precambrian sill in the Mount Shields Formation, stratigraphically above the Wallace Formation (Figure 12), yielded assemblages of epidote-actinolite-chlorite-calcite-plagioclase-quartz. The samples crystallized at a minimum pressure of 17 kPa (1.7 kb), as determined from methods outlined above, and a temperature of 350°C (Hyndman, 1985). In the youngest units of the Belt Supergroup, samples contained assemblages of muscovite-quartz, +/-plagioclase. Although the conversion to 2M polymorph muscovite can establish temperatures between 200-350°C (McMechan and Price, 1982), the 2M polymorph conversion in Belt Supergroup units occurred during Precambrian burial metamorphism (Norwick, 1972), and can not constrain temperatures reached in the Cretaceous.

Within Phanerozoic units, metamorphic minerals did not form in the Cretaceous fabric (aside from those in the contact aureole of the

Garnet stock (Minnich, 1984) and 2M mica found in slates of the Cambrian Silver Hill Formation (Babcock, 1985)). Estimates of the temperature of cleavage formation and clay mineralogy data constrain the thermal profile for units in this portion of the eastern plate. From the width of illite (001) peaks on x-ray diffraction patterns, Mitra and Yonkee (1984) estimated that cleavage formed between 130 and 200°C in rocks from thrust sheets in the Idaho-Utah-Wyoming thrust belt. Since cleavage developed in similar Mesozoic and Paleozoic carbonate and clastic rocks in this study area, this suggests that temperatures at least as high as those determined in the Idaho-Utah-Wyoming thrust belt are probably recorded in these rocks of the Montana thrust belt. A study of illite polymorphs in Paleozoic and Mesozoic rocks in the eastern plate of this study provided evidence that temperatures were, in fact, far above the minimum temperature constraints outlined above for cleavage formation. Babcock (1985) found that no samples contained lmd illite polymorph and concluded that because illite's lmd polymorph is no longer stable above 280°C (McDowell and Elders, 1980, and Jennings and Thompson, 1986), all samples reached temperatures of at least 280°C. From an increase in 2m illite polymorph in samples toward the southwest Babcock (1985) also concluded that, qualitatively, rocks underwent a greater degree of metamorphism with increasing depth of burial from the overlying western plate. The data for this portion of the eastern plate suggests a minimum temperature of 280°C in Phanerozoic rocks beneath the hangingwall plate.

To summarize changes of temperature with depth in the eastern plate, I plotted these temperatures on a schematic down-plunge projection (Figure 14). In an ideal case, the thermal boundaries of an overthrust plate should reflect the structural boundaries (Oxburgh and Turcotte, 1974). The thermal profile at a particular structural depth should be laterally continuous everywhere within the overthrust zone. For the footwall plate of this study (Figure 14), the thermal profile is clearly not laterally continuous, because down plunge, to the southeast, rocks at a given stratigraphic level recorded greater temperatures than those at the same level in the northwest. At the deeper level of the eastern plate, temperatures changed from approximately 450°C in the lower Prichard Formation to 420°C in the middle Wallace Formation. This represents a 30°C change over 5 km. At the shallower level, temperatures changed from those in the Wallace Formation to 350°C in a Precambrian sill in the Mount Shields

Figure 14. Down plunge projection (partly schematic) of the eastern plate and leading thrusts of the western plate (view 10° above horizontal in a S45E direction). V=H. Dots indicate the approximate location of samples indicative of certain temperatures. The contact aureoles of the late Cretaceous Garnet and Clinton stocks are based on mineral assemblages reported by Minnich (1984). Note that I inferred thrusts in the deepest portion of the eastern plate from thickened areas in the projection. These thickened areas may, instead, be regions of ductile shear. Shallow level thrusts are actual thrusts projected from Figure 12, with brittle fault behavior marked with open triangles and ductile fault behavior marked with wavy lines. Mz=Mesozoic Formations; Pz=Paleozoic Formations; umg=upper Missoula Group Formations (youngest to oldest; Pilcher, Garnet Range, McNamara, and Bonner); lmg=lower Missoula Group Formations (youngest to oldest; Mount Shields, Shepherd, and Snowslip). All other formations-as in Appendix A.



Formation. This represents a  $70^{\circ}\text{C}$  change over 3 km, which is a much steeper thermal gradient ( $23^{\circ}\text{C}/\text{km}$  compared with  $6^{\circ}\text{C}/\text{km}$ ). The down plunge view of the isograds therefore does not represent a thermal profile with structural depth for any particular portion of the footwall. Instead, the down plunge view highlights a lateral change in the thermal profile, with higher temperatures in corresponding levels in the southeast.

The lateral discontinuity in the footwall's thermal gradient may have resulted from changes in any of several variables (e.g. greater or lesser heat flow; higher or lower thermal conductivity), but most probably from a higher heat flow in the southeast during the period of thrusting and deformation. England and Thompson (1984) suggested that changes in heat flow from the hangingwall or changes in the hangingwall thickness may account for lateral thermal profile changes. The location of two samples with diagnostic mineral assemblages near a major thrust fault (Figure 14), might suggest that frictional heating along this fault, which lies within the eastern plate (not a leading thrust of the western plate), the Blackfoot thrust (Figure 15), raised temperatures in the southeast portion of the eastern plate. For two reasons, I discarded the possibility of frictional heating in this area. First, in a frictional heating scenario, isograds should converge from above and below toward the fault zone (England and Thompson, 1984). In this study, no evidence exists that isograds converged from below the thrust fault, though no contrary evidence exists either. A more compelling argument is that the offset on the

Blackfoot thrust (approximately 5 km (Thomas, 1987)) was insufficient for significant frictional heating, since most models suggest that offsets of at least 50 km are required for significant frictional heating (e.g. Brewer, 1981). Brewer (1981), for example, modeled 15 km thick thrust plates with a rate of movement of 5 cm/yr and a coefficient of friction of 0.6. This model required an offset of 75 km for any significant frictional heating (0.5 heatflow units) along the thrust. With the lack of evidence for isograd convergence from below the thrust fault, and the probably insufficient offset (5 km) of the Blackfoot thrust to cause frictional heating, I believe frictional heating is not a viable explanation for the increased temperatures in the southeast portion of the eastern plate. A different explanation for the increased temperatures, supported by the presence of late Cretaceous intrusives in the southeast (Wallace et al., 1987) and higher heat flow in the adjacent Flint Creek Range (Stuart, 1966), is that during the late Cretaceous, the southeastern area had a higher heat flow than rocks in the northwest. The presence of the late Cretaceous Garnet and Clinton stocks (Figure 15), the nearby Phillipsburg batholith, and late Cretaceous sills in the Sapphire Mountains to the south (Figure 15), suggest that this was a region of elevated temperatures during late Cretaceous deformation. Moreover, in the adjacent Flint Creek Range, Stuart (1966) interpreted the late Cretaceous metamorphism as Abukuma-type, low pressure-high temperature regional metamorphism. He suggested that the heat necessary for this type of metamorphism was derived from a higher heat flow in the area.

Late Cretaceous plutonic rocks in the Flint Creek Range intruded after the metamorphism (Stuart, 1966). I believe the same situation, Abukuma-type metamorphism and later plutonic emplacement, existed in the southeast portion of the eastern plate, accounting for its elevated temperatures. Similar lateral temperature variations occur in the western plate, as shown by the decrease in metamorphic grade with increasing distance from the Idaho batholith.

#### DEFORMATION STYLE AND TIMING OF LATE CRETACEOUS EVENTS

##### Western plate

At the northeast margin of the western plate, erosion exposed much of the hangingwall. Relations among late Cretaceous metamorphism, deformation, and timing are clear in this region, particularly in the well-studied Lolo Creek area (Figure 15).

The grade of M1 metamorphism in the western plate decreases with increasing distance from the Idaho batholith. In the Lolo Creek area, the grade changes from upper amphibolite in Ravalli Group rocks to biotite grade, chlorite grade, and finally unmetamorphosed rocks in the Wallace Formation, from southwest to northeast (Hall, 1968). Along the same transect, the tectonic fabrics also change.

A schematic cross-section (Figure 16) across the margin of the two plates illustrates the lateral changes in M1 metamorphism and the time and spatial relations of two fabrics that formed during the M1 and M2 thermal events. Regionally, the M1 metamorphism formed a schistosity

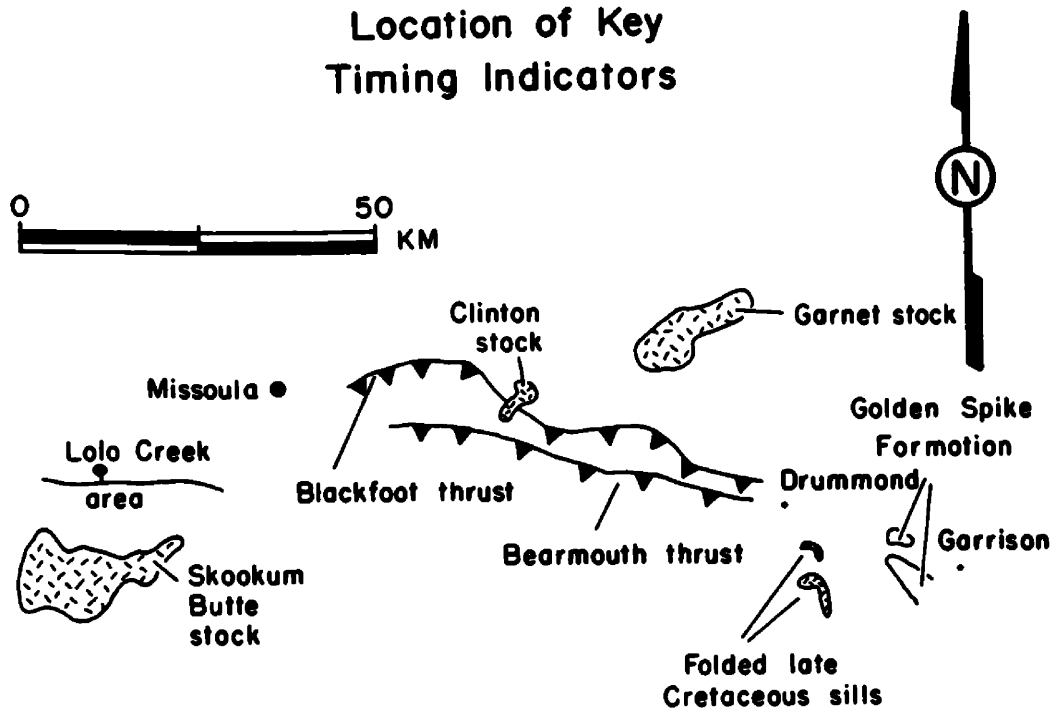


Figure 15. Location map of key indicators of deformation in the western and eastern plates.

parallel to compositional layering (Hyndman et al., 1987). This schistosity gradually fades towards the northeast, in the successively lower grade rocks (Hall, 1968) (Figure 16). A younger fabric formed during the M2 metamorphism (Rowe, 1984) and overprinted the schistosity. The younger fabric, closely associated with thrust faulting, folded the schistosity near the Idaho batholith (Hyndman et al., 1987) (Figure 16). Towards the northeast the younger fabric continues as a northeast-dipping crenulation cleavage (Rowe, 1984). Rowe (1984) found that this crenulation cleavage, which formed in rocks on the southwest side of a regional synclinorium, passes into a slaty cleavage in rocks further northeast, which lack the M1 fabric (Figure

16). With continued deformation, the slaty cleavage migrated further northeast to form the regional southwest-dipping cleavage in the eastern plate, on the northeast side of the regional synclinorium (Rowe, 1984) (Figure 16). In both plates the cleavage defines folds and lineations that plunge at a shallow angle to the southeast (Rowe, 1984). Although the regional fabric in the eastern plate crosscuts metamorphic isograds (Figure 16), the metamorphic minerals in the eastern plate formed in alignment with the fabric, during fabric formation. Thus, the eastern plate regional fabric is contemporaneous with metamorphism in the eastern plate and younger than the M1 schistosity and M1 metamorphism of the western plate.

Contact metamorphism in rocks of the Lolo Creek area establishes a younger age limit for the crenulation cleavage in the western plate and associated regional cleavage in the eastern plate. Rowe (1984) found randomly oriented biotite that overgrew the crenulation cleavage in the Wallace Formation of the Lolo Creek area. The biotites apparently grew as part of a contact metamorphic assemblage from the nearby Skookum Butte stock, south of Lolo Creek (Figure 15). The Skookum Butte stock, related to the main mass of the Idaho batholith, is more mafic (Don Hyndman, personal communication) than the main mass (dated at 70-75 Ma) (Criss and Fleck, 1987), and probably is at least as old or older than the main mass (Don Hyndman, personal communication). Because the Skookum Butte stock's contact assemblage overprints the crenulation cleavage, the crenulation cleavage and associated eastern plate regional fabric are older than 70-75 Ma (Figure 6). The relationships

between regional cleavage and late Cretaceous formations and intrusions in the eastern plate also bracket the age of the regional cleavage.

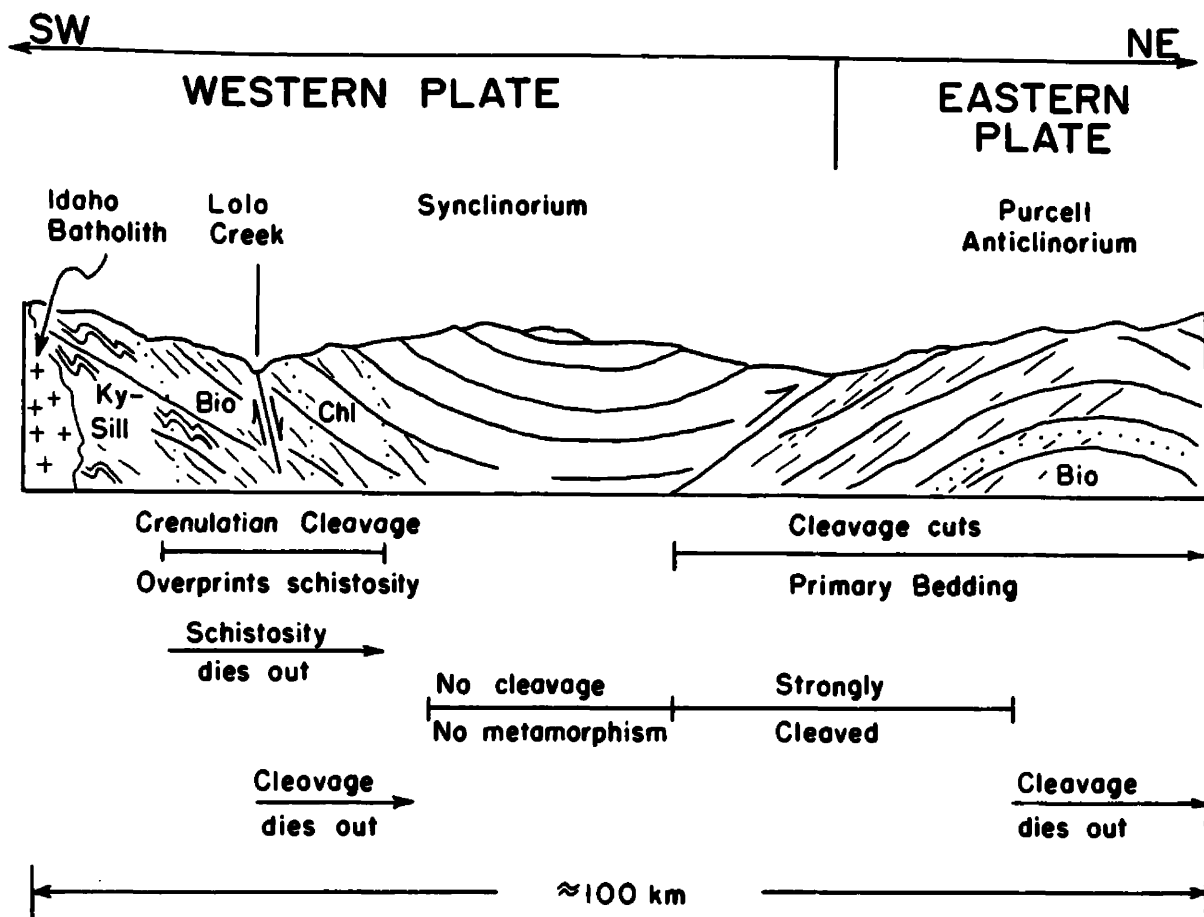


Figure 16. Schematic section through the Lolo Creek area showing relationships of M1 metamorphism and M1 and M2 fabrics of the western plate to the regional fabric and metamorphism of the eastern plate.

### Eastern plate-Deformation style

The regional fabric varies in intensity throughout the eastern plate as a function of lithology, proximity to faults, and burial depth, and exhibits some changes in orientation due to later rotation by normal faults. Broad open folding and simple shearing (as

determined from deformed sandstone dikes and pyrite pressure shadows, described below) deformed the deepest levels of the eastern plate. Strain within certain units is considerable (e.g. maximum elongation values ranging from 2.4 to 10.0 in the lower Prichard Formation). Shallower levels deformed by tight folding and thrust faulting, though some units reponded in local areas (e.g. adjacent to thrust faults and in the cores of tight folds) by deforming ductilely. At shallower levels, Tertiary normal faults rotated the regional fabric away from its average southwest dip in some structural blocks.

Although several units at the deepest level of the footwall plate probably underwent ductile deformation, only one unit, the upper Prichard Formation, contains measurable indicators of strain. In rocks of the upper Prichard Formation, pyrite pressure shadows and deformed sandstone dikes (Figures 17, 18, and 19) enabled me to estimate the strain. The rotated sandstone dikes (Figure 19) and pyrite pressure shadows (Figures 17 and 18) suggest that this level of the eastern plate underwent simple shear.

To estimate the strain in the pressure shadows, I used methods outlined in Ramsay and Huber (1983). Appendix D contains all strain data from the pressure shadows and deformed sandstone dikes. Because of the geometry of the pressure shadows and their alignment with the regional cleavage, I assumed homogeneous, plane strain (Ramsay and Huber, 1983). The strain was homogeneous, since the shape of the pyrite pressure shadows was constant throughout all samples studied. The lack of quartz fiber growth in the y-direction in the pyrite



Figure 17. Photomicrograph of pyrites with pressure shadows aligned with the late Cretaceous fabric in the upper Prichard Formation, sample 34. Field of view is 3.5 mm.



Figure 18. Close-up of Figure 17, with field of view of 1.0 mm.

pressure shadows, as determined from thin-section analysis, suggests the condition of plane strain. I did not assume constant volume, because I found evidence for volume loss in the geometries of the sandstone dikes and pyrite pressure shadows (Figures 17, 18, and 19). The volume loss may have resulted from dehydration reactions during prograde metamorphism (Hyndman, 1985) in the eastern plate. If so, significant shortening during deformation by simple shear in the deeper levels of the eastern plate may be attributed to this volume loss. Within the confines of these conditions, I determined the maximum elongation (X) from the pressure shadows by using (1 + principle elongation), where the principle elongation is defined as fiber length/pyrite radius. In addition, I measured fiber lengths and pyrite radii in thin sections cut orthogonal to the fabric (Appendix D), although I could not use these values to define the strain ellipsoid, given the probable volume loss. The values of X from pressure shadows in the upper Prichard Formation ranged from 2.4 to 10.0, with an average of 5.2. The average value of X in each of the seven samples ranged from 3.0 to 7.0. Possible errors in the estimation of X include 1) the difficulty of measuring large strains accurately, since mineral aggregates (quartz, here) lose definition with the onset of banding and 2) the tendency of mineral aggregates with large strain values to thin towards the higher strain end (Simpson, 1983). In spite of these possible sources of error, the geometry of the pressure shadows (Figure 18) still requires high strain (Selkman, 1983).

Another indicator of high strain in the upper Prichard Formation

came from measurements of four deformed sandstone dikes in sample 54 (Figure 19). The average shear strain value for the dikes was 3.5

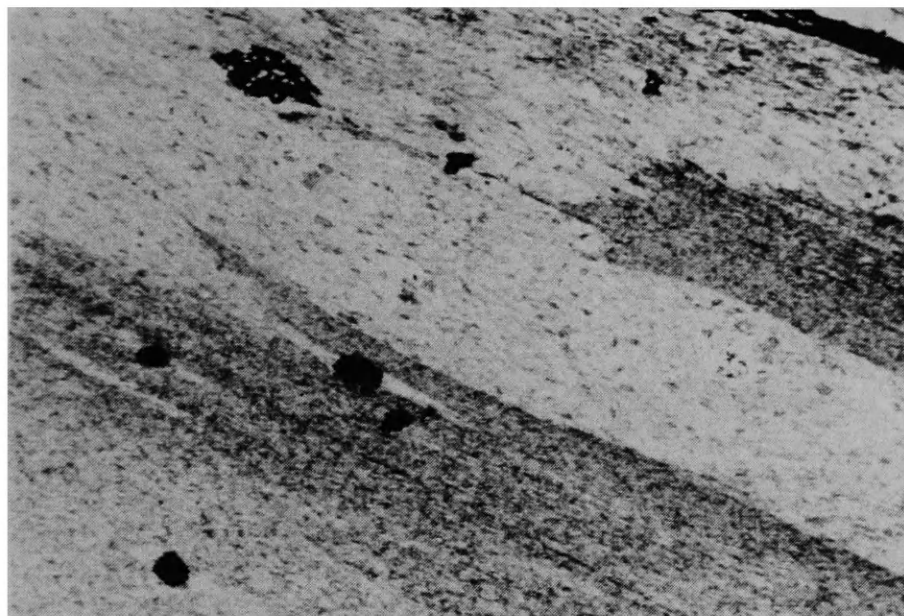


Figure 19. Photomicrograph of a deformed sandstone dike aligned with the regional fabric, 24 degrees from bedding (horizontal), from sample 54, upper Prichard Formation. Field of view is 3.5 mm.

(Appendix D). I based my assumption that the sandstone dikes were originally perpendicular to bedding on work done by Shelton (1961) and Borradaile (1984). With the small sample size (four), the average shear strain value is not statistically significant (Borradaile, 1984), but because the sandstone dikes rotated 70 degrees, they show qualitatively a high shear strain (Borradaile, 1984). Sample 54 also contained pyrite pressure shadows (Figure 19). A sketch map and projection to a sketch of the thin section (Figure 20) illustrate field relations for sample 54. The sense of shear for the deformed sandstone

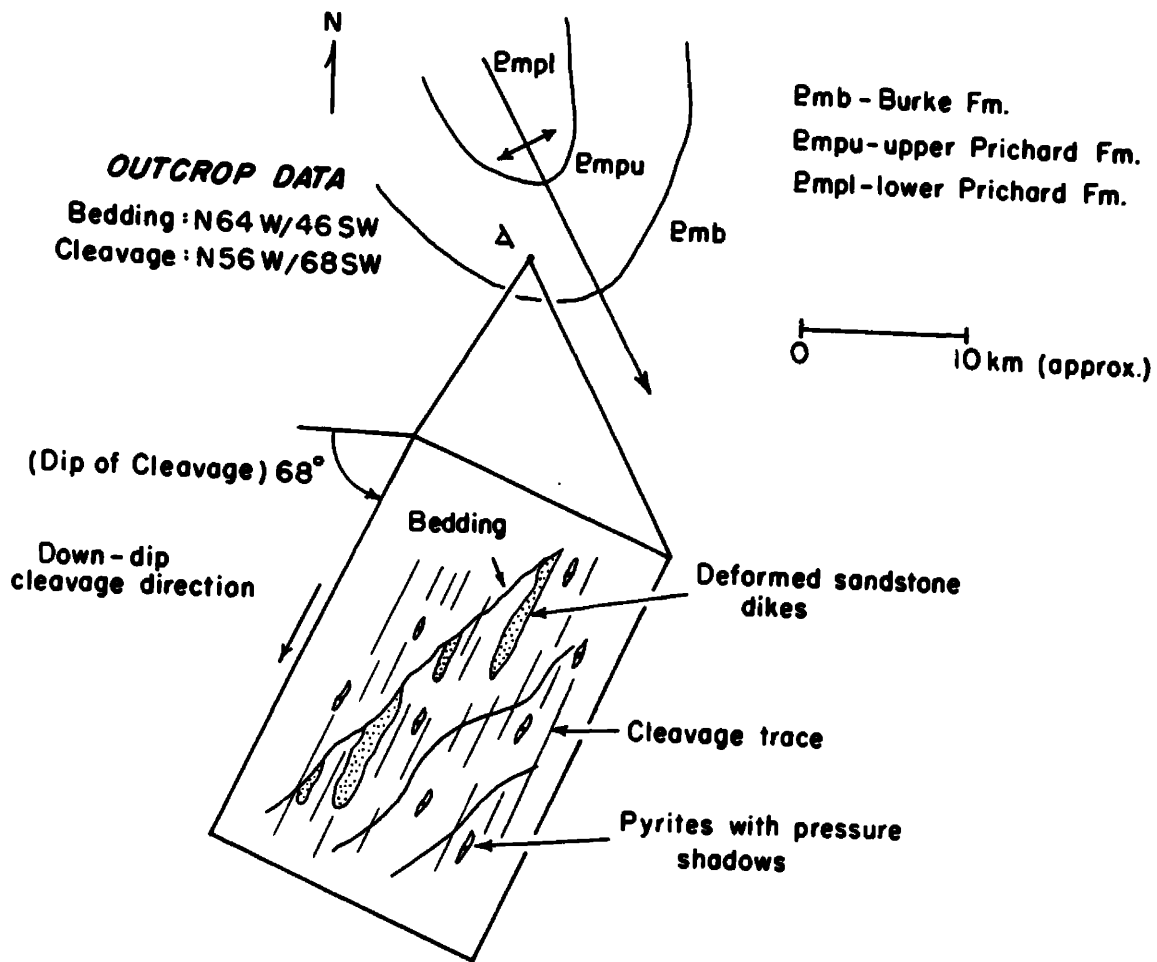


Figure 20. Sketch map indicating field relations for sample 54 (upper Prichard Formation) and a projection to a thin-section. The northeast sense of shear for the pressure shadows and deformed sandstone dikes in the thin section matches the late Cretaceous thrusting direction.

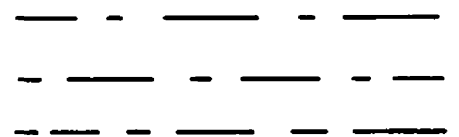
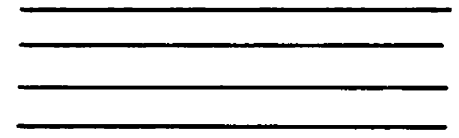
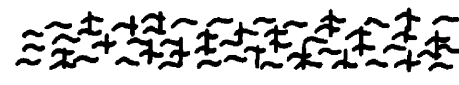
dikes matches that for the pyrite pressure shadows. The sense of simple shear (top to the northeast) also agrees with the thrusting direction of the western, hangingwall plate. Shear strain values and maximum elongation values indicate that this portion of the footwall plate underwent considerable shortening by penetrative, simple shear.

The maximum elongation values in the footwall plate are larger

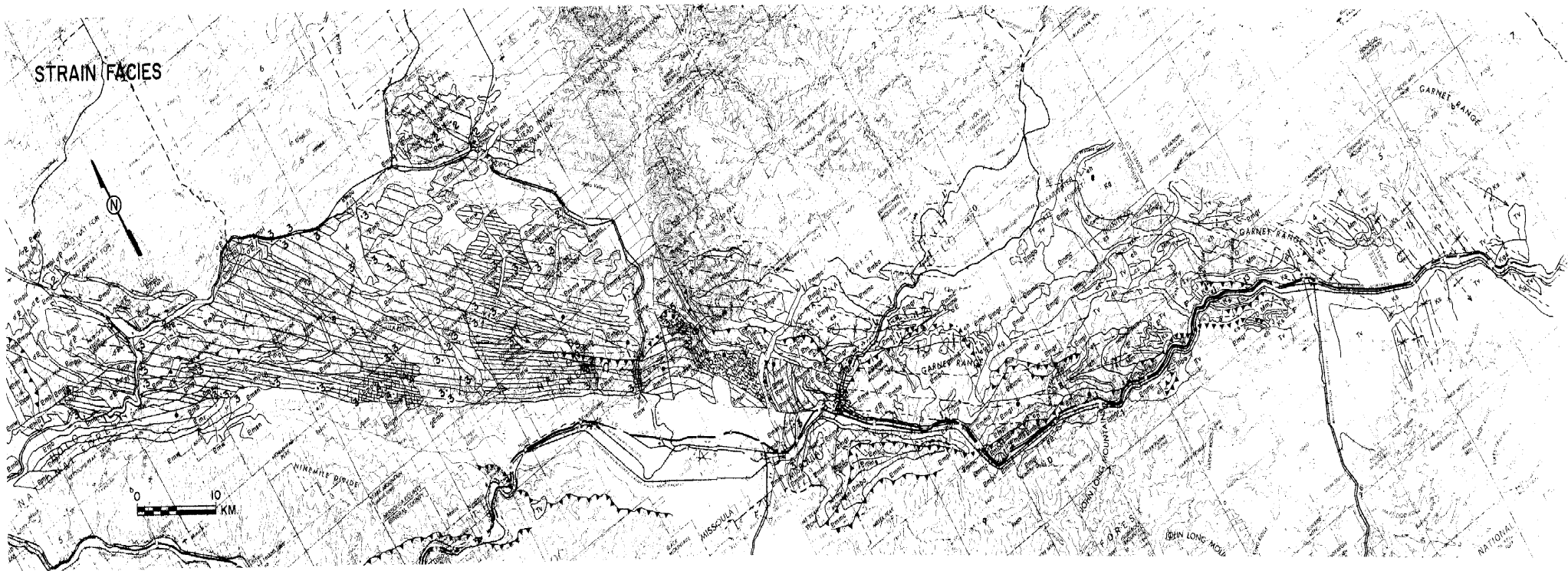
than those reported in many other areas of greenschist metamorphism. From pyrite pressure shadows in rocks of the Southern Appalachians, Reks and Gray (1983) determined X values of 1.13 to 2.14, while Siddans et al. (1984) reported X values of 1.17 to 3.30 for Permian rocks of the Alpes Maritimes in France. Values reported by Harper (1968) for the Taconic slate belt of New York and Vermont are higher; average X = 4.17. Like the Taconic slate belt, the upper Prichard Formation, deep in the footwall plate, shortened more by ductile deformation than units at higher, cooler levels in the plate.

At the higher, cooler levels of the eastern plate, units shortened by thrust faulting and tight folding. However, some units did undergo ductile deformation, particularly near major thrust faults. Two samples from the Mount Shields Formation contained strain indicators (data in Appendix D). Pyrite pressure shadows from sample 119 (Figure 11) gave an average maximum elongation of 2.5, while deformed sandstone dikes from sample 129 (Figure 11) had an average shear strain value of 0.90. Both values are lower than corresponding values from the deeper level, upper Prichard Formation. A map of "strain facies" (Figure 21) prepared from my data and that of Dr. James Sears, illustrates another difference in deformation style between deeper and shallower levels in the eastern plate. The strain facies map (adapted from descriptions of characteristics of increasing strain in Ramsay and Huber, 1983) assigns higher numbers to areas of higher strain, based on characteristics visible at the outcrop (for example, all areas with a phyllitic sheen on the cleavage surface of pelitic layers and spaced cleavage in

Figure 21. Strain facies map shows the cleavage orientation and relative intensity using the following zone designations. In general, the more closely-spaced the lines, the greater the recorded strain in the rocks. Note that all changes of strain intensity are gradational, as are the symbols used. Dots and numbers indicate strain observation points.

<u>Zone</u>	<u>Symbol</u>	<u>Characteristics</u>
1		spaced cleavage, pencil cleavage, tension gashes, slickensides, small-scale folds and thrusts
2		continuous slaty cleavage in pelitic layers, no slickensides, minor tension gashes, and no small-scale thrusts
3		phyllitic cleavage in pelitic layers, spaced cleavage in quartzites
4		strong stretching lineation on phyllitic cleavage, closely spaced cleavage in quartzites
5		bedding transposed to cleavage, sheath folds, mylonites

STRAIN FACIES



quartzite layers require a zone 3 designation). Each strain zone designation corresponds to a certain map pattern (Figure 21). The map patterns, oriented with the cleavage trend, are widely-spaced in areas of low strain facies values (e.g. in zone 1, where pelitic layers contain spaced cleavage) and closely-spaced in areas of high strain facies values (e.g. in zone 5, where rocks have mylonitic textures). In zones 4 and 5, short bars perpendicular to the cleavage trend represent stretching lineations in highly strained rocks. The areas of higher strain in deeper levels of the footwall follow the boundaries of formations, indicating that the strain was not due to a local source (e.g. a thrust fault), but rather, due to regional conditions (Woodward et al., 1985). The strain is concentrated in the weaker, pelitic units (e.g. the upper Prichard Formation) and not in the stronger, quartzite units (e.g. Revett Formation). Woodward et al. (1985) also found a concentration of strain in rheologically weaker units in examples from the Valley and Ridge Province in southwestern Virginia. Strain concentration based solely on the rheology of the formation did not occur at shallower levels in the footwall. Instead, the occurrence of ductile deformation seemed to depend more on the distance from a major thrust (Figure 21). Zones of decreasing strain facies generally occurred away from major thrusts. Overall, the shallower levels contain a lesser areal extent of higher strain facies than deeper levels of the footwall (Figure 21), due to increased shortening by thrusting and folding.

Leading thrusts that placed the western plate over the eastern

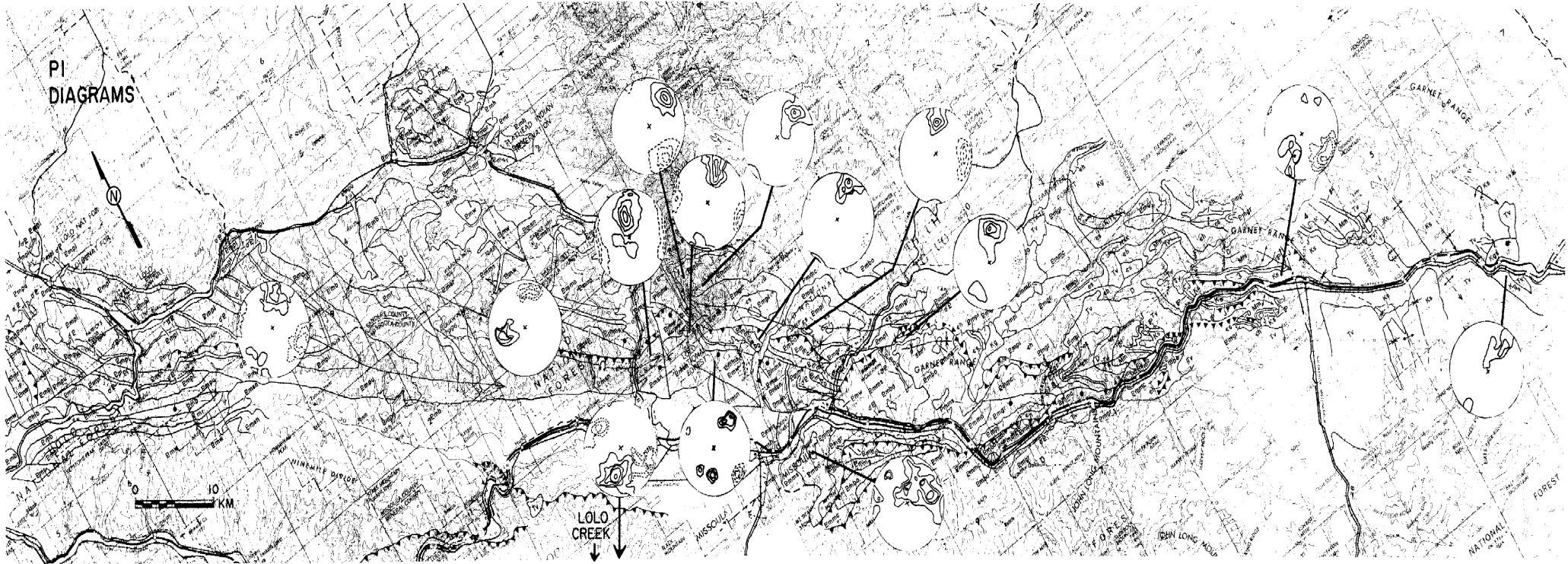
plate and thrusts within the eastern plate (with much less offset) vary considerably with respect to their strain facies values. A schematic down plunge view of these thrusts (Figure 14) illustrates that while many thrusts behaved brittle in a manner (low strain facies values), others were associated with ductile deformation (high strain facies values). The difference in behavior of adjacent thrusts is probably due to the time each thrust moved during progressive deformation. The leading thrusts that placed the western plate over the eastern plate acted brittlely, since (assuming no frictional heating) during and immediately after thrusting, temperatures in the overthrust eastern plate remained low (Oxburgh and Turcotte, 1974). After the western plate thrust over the eastern plate, temperatures rose in the eastern plate, equilibrating with the new conditions (Davy and Gillit, 1986). Later thrusts, within the eastern plate, which moved after most of the equilibration of the isograds, were associated with ductile deformation. For example, the Blackfoot thrust, near Bonner, Montana (Figure 21, 10 km east of Missoula) contained mylonite, and probably moved later than the leading thrusts of the western plate, south of Bonner, which moved in a brittle manner, without ductile deformation. The difference in behavior during movement, of leading thrusts of the western plate and later thrusts within the eastern plate, becomes less at shallower levels in the down plunge direction, to the southeast. The thrusts within the eastern plate, at progressively shallower levels, cut stratigraphically higher, cooler rocks, similar to rocks cut earlier by leading thrusts of the western plate (Figure 14).

In the shallower levels of the eastern plate, a few regions have lineations oriented away from the normal southeast plunge of the regional fabric (Sears et al., 1985). Figure 22 includes Pi diagrams of lineation and cleavage plane orientation measurements from different areas within the panel of the regional cleavage. In some areas, for example the Jocko Mountains north of Missoula, Montana (Figure 22), the fabric underwent a clockwise rotation. This resulted from Tertiary normal faulting, associated with the Lewis and Clark line, that rotated some structural blocks (Watson, I.A., 1984, Sears et al., 1985, and Ort, in progress). Sears and coauthors (1985) determined that normal faults clearly rotated the blocks after the late Cretaceous thrusting and cleavage formation.

#### Eastern plate-Timing of late Cretaceous events

Cross-cutting relations and regional plutonic rocks tightly bracket the time of thrusting and cleavage formation in the eastern plate. The cleavage deforms the late Cretaceous Golden Spike Formation, near Garrison, Montana (Figure 15). Late Cretaceous sills in the Sapphire Mountains to the south (Figure 15) folded during deformation. The emplacement of the late Cretaceous Garnet stock (Figure 15) was contemporaneous with the regional cleavage formation, while the Clinton stock (Figure 15) crosscut a thrust during its emplacement. Finally, a late Cretaceous stock near the Boulder Batholith crosscuts the cleavage (James Sears, personal communication). All indicators agree that the deformation was late Cretaceous.

Figure 22. Map of Pi diagrams. Each diagram contains poles to cleavage (solid contours) and, where data was available, bedding/cleavage lineations (dashed contours or dot locations). The contours in most areas indicate a southeast plunge, except those rotated by Tertiary normal faulting (e.g. north and east of Missoula, Montana).



The cleavage crosscuts the late Cretaceous Golden Spike Formation, described as a syntectonic conglomerate with a western source, interlayered with volcanic rocks (Gwinn and Mutch, 1965, and Mackie, 1986). The volcanic rocks of the Golden Spike Formation correlate with the Elkhorn Mountains Volcanics further east (Mackie, 1986). The Boulder batholith, in turn, intrudes the Elkhorn Mountains Volcanics (Gwinn and Mutch, 1965). Baadsgaard and coauthors (1961) dated the Marysville stock (Figure 15), a satellite pluton of the Boulder batholith. Potassium/argon ratios from biotites yielded ages of 78-82 Ma. In addition, fossils at the base of the Carter Creek Formation, underlying the Golden Spike Formation, were estimated as 88 Ma old (Gwinn and Mutch, 1965). The Elkhorn Mountains Volcanics and Golden Spike Formation are older than the 78-82 Ma Marysville stock, and younger than the 88 Ma date of the base of the Carter Creek Formation. The regional cleavage which cuts the Golden Spike Formation is younger than 82 Ma (Figure 6). Because the 1,219-2,438 meters thick Golden Spike Formation contains distinctive reddish quartzite pebbles, probably of the Proterozoic Bonner Formation (Gwinn and Mutch, 1965), the overthrust hangingwall plate had eroded down to the level of the Bonner Formation before the cleavage deformed the Golden Spike Formation. Relations with regional plutons, also in the southeast portion of the footwall plate, further constrain the ages of deformation.

Late Cretaceous plutonic rocks which provide timing constraints include sills which folded during deformation, a stock that intruded

during cleavage formation, a stock which crosscut a late Cretaceous thrust fault, and a stock that overgrew the cleavage. Late Cretaceous sills in the Sapphire Mountains to the south (Figure 15) loosely bracket the time of deformation. These sills intruded from approximately 97-80 Ma and folded during deformation together with the overlying Cretaceous strata (Wallace et al., 1987). The Garnet stock (Figure 15) more tightly constrains the time of deformation, since it intruded during cleavage formation (Minnich, 1984). Minnich (1984) found that cordierites from the contact aureole of the Garnet stock overgrew cleavage, grew contemporaneously with cleavage formation, and later underwent rotation from cleavage formation. An 82 Ma potassium/argon date from hornblende for the Garnet stock (Ruppel et al., 1981) suggests cleavage formed at least during emplacement at 82 Ma (Figure 6). Similarities between the Garnet stock and Clinton stock (Figure 15) suggest that they were part of a single magmatic pulse (Thomas, 1987). If so, the Clinton stock probably intruded at approximately 82 Ma, as well. Because the Clinton stock crosscuts the Blackfoot thrust (Thomas, 1987), the Blackfoot thrust is older than 82 Ma. Moreover, since ductile deformation accompanied the portion of the Blackfoot thrust near the Clinton stock, it probably moved later than brittle thrusts, as described above. Consequently, most thrusting, including the major, brittle thrusts that placed the western plate over the eastern plate, occurred before 82 Ma (Figure 6). A radiometric age date from an unnamed stock near the Boulder batholith brackets the youngest possible age for deformation and cleavage formation. McDowell

(1971) dated a stock (number 409 from Daniel and Berg, 1981) at 73 Ma (Figure 6), using potassium/argon ratios from biotite. This stock crosscuts the regional cleavage (James Sears, personal communication). Age dates from late Cretaceous sills and stocks agree with estimated ages of deformation determined from the Golden Spike Formation. Because timing constraints from both plates concerning the age of metamorphism and deformation agree well (Figure 6), they enabled me to describe a sequence of events for the region during the late Cretaceous.

#### GEOLOGIC HISTORY

During the middle to late Cretaceous, a combination of heating, associated with pluton emplacement, and thrusting produced the maximum thermal profiles recorded in the western and eastern plates (Figure 23). The western plate (Figure 23) contains a Barrovian sequence (Hietanen, 1984), up to upper amphibolite grade, of Belt Supergroup rocks heated during the early stages of emplacement of the Idaho batholith. In the eastern plate distinct thermal profiles formed in the northwest and southeast regions (Figure 23). Deeper level rocks exposed in the northwest region underwent considerable shortening from ductile deformation, but only reached temperatures in the biotite zone. Conversely, shallower level rocks in the southeast deformed more by thrusting and folding than by ductile deformation. Yet, temperatures in that portion were considerable, even in stratigraphically high

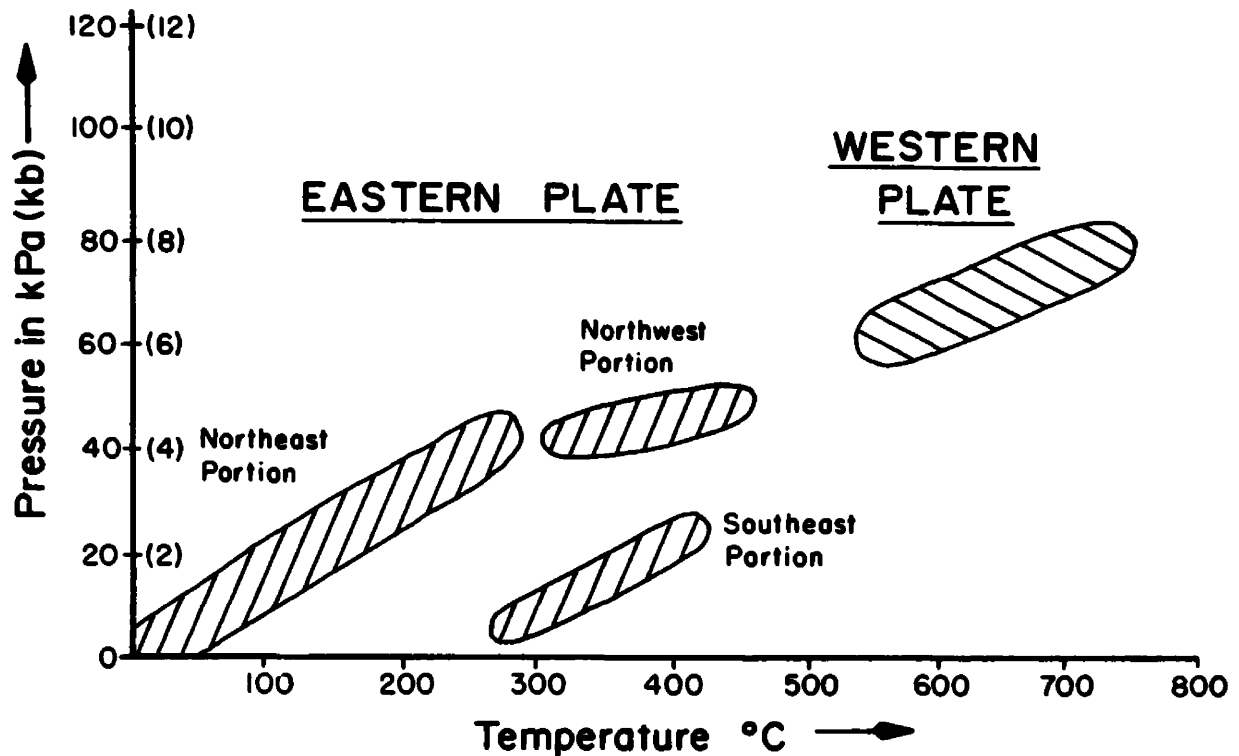


Figure 23. A pressure-temperature diagram of preserved thermal profiles from the western plate and different portions of the eastern plate. The profile for the northeast portion of the eastern plate is approximate.

levels (e.g. approx. 280°C in Cretaceous strata). The greater recorded temperatures probably reflect a higher regional heat flow, as evidenced from the intrusion of Cretaceous plutons, such as the Garnet and Clinton stocks. Northeast of the overthrust zone (Figure 23, approximate thermal profile), but still in the eastern plate, rocks as deep as the Prichard Formation lack well-developed cleavage and did not reach temperatures in the chlorite zone; these rocks lacked the added heat caused, in part, by burial beneath the western, hangingwall plate.

By themselves, the thermal profiles mean very little, but together with information on structures, fabrics, and crosscutting relations, they outline the following sequence of middle to late Cretaceous events in western Montana and eastern Idaho.

#### 105-95 Ma

Transform faulting ceased at the former western continental border at 105 Ma (Lund and Snee, 1985). Folding and thrusting from continental accretion deformed the Wallowa-Seven Devils terrane (Lund and Snee, 1985). Early quartz diorites and tonalites of the Idaho batholith intruded at 100 Ma, beginning the M1 event later preserved in the border zone of the Idaho batholith (Toth, 1987). In the eastern plate, sills intruded into Cretaceous rocks beginning at 97 Ma.

#### 95-85 Ma

Deformation at the continental margin shifted from the terrane to the suture zone with the former western continental border (Lund and Snee, 1985 and Criss and Fleck, 1987). More quartz diorite and tonalite of the Idaho batholith (Toth, 1987) intruded and rocks of the future Idaho batholith border zone continued heating from the M1 event until 85 Ma (Lund and Snee, 1985), when most tonalite emplacement ceased. Layer-parallel schistosity developed in rocks coevally with M1 metamorphism (Hall, 1968). At 87 Ma suture zone plutons began to intrude and close the suture (Criss and Fleck, 1987), though these were highly strained from continued deformation in the suture zone. In the

eastern plate, sediments at the base of the Carter Creek Formation had been deposited by 88 Ma (Gwinn and Mutch, 1965), while sills continued to intrude into Cretaceous strata.

85-82 Ma

The western plate, thickened from pluton emplacement and deformation from continental suturing, failed by thrusting or gravitational spreading to the northeast, over the eastern plate. Highly strained plutons that continued to close the suture zone (Criss and Fleck, 1987), cooled quickly after the unroofing of at least 7 km of overburden. Further east, rapid cooling accompanied uplift in the area that would later contain the Idaho batholith (Lund and Snee, 1985). The second thermal event in the western plate, M2, formed lower pressure and temperature mineral assemblages, due to the decreased overburden, and formed a new fabric. The new fabric, a crenulation cleavage, folded and overprinted the layer-parallel schistosity in rocks near the present-day Idaho batholith (Rowe, 1984 and Hyndman et al., 1987).

The thrust and rapidly-eroding western plate shed sediments (including pebbles of the Proterozoic Bonner Formation) into the eastern plate, that interfingered with volcanics of the Elkhorn Mountains Volcanics to form the 1,219-2,438 meter thick Golden Spike Formation, a syntectonic conglomerate (Gwinn and Mutch, 1965, and Mackie, 1986). Thrusting of the western plate over the eastern plate occurred before emplacement of the Clinton stock, at approximately 82

Ma (Thomas, 1987).

82-79 Ma

Plutons in the suture zone continued to close the suture (Criss and Fleck, 1987). Just east of the suture zone, plutons continued to cool quickly (Criss and Fleck, 1987), as did rocks in the Idaho batholith complex (Lund and Snee, 1985). The fabric formed during M2 metamorphism began to deform rocks further to the northeast, defining a southeast-plunging fold system and becoming the regional fabric of the eastern plate (Rowe, 1984).

The regional fabric formed in the eastern plate, defining a southeast-plunging fold system correlative with that in the western plate. Deeper levels in the footwall plate formed broad folds and deformed by simple shearing, with strain concentrated in the weaker, pelitic formations. Temperatures of 450-525°C enabled biotite and chlorite to grow in the fabric. At shallow levels, rocks thrust and formed tighter folds in sedimentary rocks as young as the Golden Spike Formation and in late Cretaceous sills. Ductile deformation at shallow levels was confined to areas near thrusts, and was largely independent of the formation present. Temperatures in the southeast portion of the footwall plate were higher than those at the same structural levels in the northwest. Higher heat flow, as evidenced from late Cretaceous plutons such as the Garnet and Clinton stocks, may have raised the temperatures. The Garnet stock, dated at 82 Ma, cooled contemporaneously with the cleavage formation.

79-present

In the western plate, near the Lolo Creek area (Figure 15), the contact metamorphic assemblage of the Skookum Butte stock had overgrown the crenulation cleavage by 75-70 Ma ago (Criss and Fleck, 1987, and Don Hyndman, personal communication). A stock near the Boulder batholith, dated at 73 Ma (McDowell, 1971), crosscut the regional fabric in the eastern plate. Later, the eastern plate overrode Paleocene deposits in the Montana disturbed belt, carrying the western plate with it (Sears, 1985). In shallower areas of the eastern plate, normal faults rotated the regional fabric in a clockwise direction (Sears et al., 1985). Erosion later exposed much of the eastern and western plates.

#### SUMMARY

The thrusting and reequilibration of isograds in the thrust plates of this study correspond well, overall, with values reported from thermal models. Conditions during thrusting of the western plate mimic those in models, but after thrust emplacement and reequilibration of the isograds, the maximum temperatures reached at various stratigraphic levels in the southeast portion of the eastern plate are significantly higher than those predicted from thermal modeling.

During thrusting, the western plate moved, at a rate comparable

to those used in thermal models, over thrusts that behaved brittlely in the initially cool rocks. Maps along the zone of thrusting (e.g. Nelson and Dobe1, 1962, Hall, 1968, Desormier, 1975, and Wallace, et al., 1987) show that the Wallace Formation is the oldest unit exposed in the hangingwall rocks of leading thrusts of the western plate. This indicates that the decollement which placed the western plate over the eastern plate rests in the Wallace Formation. The hangingwall plate thus ranged between 8 km (excluding Mesozoic rocks) and 12 km (including all Mesozoic rocks except the Golden Spike Formation) thick. This plate moved approximately 50 km (Sears, 1986) from approximately 85 to 82 Ma (Figure 6) at a minimum speed of 1.7 cm/year. Though somewhat lower, this rate of movement compares reasonably well with Oxburgh and Turcotte's (1974) reported value of 3.0 cm/year, which they based on the plate tectonic rates. As the plate moved, the Bearmouth thrust (Figure 15) and leading thrusts of the western plate acted brittlely (Figure 22) in rocks that largely retained their pre-thrusting thermal gradient. After thrust emplacement, initial pressures in the footwall increased by 3-4 kb, just as thermal models predict (e.g. England and Richardson, 1977, England and Thompson, 1984, and Davy and Gillit, 1986). After isostatic loading of the crust by the thrust plate, the large pressure increase may have contributed (Mackie, 1986) to the formation of the basin for the 1,219-2,438 meter thick Golden Spike Formation (Gwinn and Mutch, 1965).

After thrusting, the western plate eroded, at a rate comparable to those used in thermal models, to form the Golden Spike Formation. The

Golden Spike Formation, with deposition bracketed between 88–82 Ma (Figure 6) is probably not older than 85 Ma, since thrusting did not begin until about that time (Figure 6). Since the Golden Spike Formation contains pebbles of the Proterozoic Bonner Formation, the western plate eroded about 4.5 km (not including Mesozoic rocks) during the span of deposition of the Golden Spike Formation, between 85 and 82 Ma. This minimum value for the rate of erosion, 1.5 mm/year, falls within geologically conservative rates (0.1–1.7 mm/year) used by England and Thompson (1984) in their modeling. As the western plate eroded, depositing the Golden Spike Formation, isotherms rose in the footwall, and thrusts that moved after the reequilibration (e.g. the Blackfoot thrust, within the eastern plate (Figure 15)) were associated with ductile deformation (Figure 22). Unlike isotherms in thermal models for overthrusting, the isotherms in this study did not rise to the same structural levels in all parts of the overlap zone.

Within rocks of the southeast portion of the overlap zone, higher temperatures than those at similar structural levels in the northwest may have resulted from higher late Cretaceous heat flow in the southeast, since a thermal model predicts lower maximum temperatures than those actually preserved in the rocks. The actual temperature preserved in sample 128 from the Wallace Formation, at a depth of 8 km below the leading thrusts of the western plate (Figure 14), was a minimum of 420°C. For samples 130 and 131 from a Precambrian sill in the Mount Shields Formation, at a depth below the western plate of 5 km, the actual temperature preserved was 350°C. For samples 8 and 5 km

beneath a 15 km thick thrust plate (probably somewhat thicker than the hangingwall plate in this study), assuming a geothermal gradient of 30° C/km, Oxburgh and Turcotte's (1974) model predicts maximum temperatures of 370 and 240°C, respectively. The prediction by a thermal model (assuming the model is reasonably accurate and applicable to this study) of temperatures lower than those actually determined in rocks, provides evidence that overthrusting alone, in the southeast portion of the eastern plate, is insufficient to account for the higher recorded temperatures. In such cases, England and Thompson (1984) suggested that an increase in the supply of heat from the mantle probably accounts for the higher temperatures. In their study of the Eastern Alps, Oxburgh and Turcotte (1974) found that it was difficult to explain the metamorphic conditions in the overthrust Eastern alps without an anomalously high heat flow from the mantle. In this study, higher heat flow from the mantle may also be a reasonable conclusion, because of the low pressure-high temperature metamorphism in the adjacent Flint Creek Range, which preceded the emplacement of plutons in the area (Stuart, 1966). Presumably, similar conditions (i.e. Abukuma-type metamorphism, then emplacement of plutons) may have existed in the southeast portion of the eastern plate during thrusting in the late Cretaceous. In this area, it might be interesting to try to take out the effects of the higher regional heat flow to estimate the true thermal effects of the thrust faulting.

## REFERENCES

- Agevine, C.L., and D.L. Turcotte, 1983, Oil generation in overthrust belts: AAPG Bulletin, v. 67, p. 235-241.
- Baadsgaard, H., Folinsbee, R.E., and J. Lipson, 1961, Potassium-argon dates of biotites from Cordilleran granites: Geol. Soc. Am. Bull., v. 72, p. 689-702.
- Babcock, W.H., 1985, Mineralogic features of tectonic loading associated with the Bearmouth thrust: unpublished senior thesis, Univ. of Montana, 13 p.
- Borrodaile, G.J., 1984, A note on sand dyke orientations: J. Struc. Geo., v. 6, p. 587-588.
- Bostick, N.H., 1974, Phytoclasts as indicators of thermal metamorphism, Franciscan Assemblage and Great Valley sequence (Upper Mesozoic), California: in Carbonaceous materials as indicators of metamorphism, Geol. Soc. Amer. Spec. Paper 153, p. 1-17.
- Brewer, J., 1981, Thermal effects of thrust faulting: Earth and Planetary Science Letters, v. 56, p. 233-244.
- Carey, J.W., and J.M. Rice, 1985, Petrology and metamorphic history of metapelites in the Boehls Butte Quadrangle, norther Idaho: Geol. Soc. Am. Bull. Abstracts with Programs, v. 17, p. 539.
- Chase, R.B., 1973, Petrology of the northeast border zone of the Idaho batholith, Bitterroot Range, Montana: Montana Bureau of Mines and Geology Memoir 43, 28 p.
- Chase, R.B., and B.R. Johnson, 1977, Border-zone relationships of the northern Idaho batholith: Northwest Geology, v. 6, p. 38-50.
- Childs, J.F., 1982, Geology of the Precambrian Belt Supergroup and the northern margin of the Idaho batholith, Clearwater County, Idaho: Ph.D. Dissertation, University of California, Santa Cruz.
- Cliff, R.A., 1985, Isotopic dating in metamorphic belts: J. Geol. Soc. Lond, v. 142, p. 97-110.
- Cook, F.A., 1983, The effect of a lateral deformation on heat flow-heat production relations: Can. J. Earth Sci., v. 20, p. 1621-1630.
- Crawford, M.L., and L.E. Mark, 1982, Evidence from metamorphic rocks for overthrusting, Pennsylvania Piedmont, U.S.A.: Can. Min., v. 20, p. 333-347.

- Criss, R.E., and R.J. Fleck, 1987, Petrogenesis, geochronology, and hydrothermal systems of the northern Idaho batholith and adjacent area: U.S.G.S., Prof. Paper 1436, p. 95-137.
- Daniel, F., and R.B. Berg, 1981, Radiometric dates of rocks in Montana: Montana Bureau of Mines and Geology, Bulletin 114, 136 p.
- Davis, D., Suppe, J., and F.A. Dahlen, 1983, Mechanics of fold-and-thrust belts and accretionary wedges: J. Geo. Res., v. 88, p. 1153-1172.
- Davy, Ph. and Ph. Gillit, 1986, The stacking of thrust slices in collision zones and its thermal consequences: Tectonics, v. 5, p. 913-929.
- Desormier, W.L., 1975, A section of the northern boundary of the Sapphire tectonic block: master's thesis, Univ. of Montana, 64 p.
- England, P.C., and S.W. Richardson, 1977, The influence of erosion upon the mineral facies of rocks from different metamorphic environments: J. Geol. Soc. Lond., v. 134, p. 201-213.
- England, P.C., and A.B. Thompson, 1984, Pressure-temperature-time paths of regional metamorphism I. Heat transfer during evolution of regions of thickened continental crust: J. of Petr., v. 25, p. 894-928.
- Griffin, J., in progress, Structural style of Mesozoic rocks, Garnet Range Subplate, Montana: master's thesis, Univ. of Montana.
- Gwinn, V.E., 1961, Geology of the Drummond area, central-western Montana: Montana Bureau of Mines and Geology, Spec. Publ. 21, Geologic Map 4.
- Gwinn, V.E., and T.A. Mutch, 1965, Intertongued upper Cretaceous volcanics and nonvolcanic rocks, central-western Montana: Geol. Soc. Am. Bull., v. 76, p. 1125-1144.
- Hall, F.W., 1968, Geology of the north half of the Missoula 30' quadrangle: Ph.d. dissertation, Univ. of Montana, 166 p.
- Harper, C.T., 1968, Isotopic ages from the Appalachians and their tectonic significance: Can. J. Earth Sci., v. 5, p. 49-59.
- Harris, A.G. 1981, Color and alteration: an index to organic metamorphism in conodont elements: in Treatise on Invertebrate Paleontology, Part W, Miscellanea (Supplement 2), Conodonts, Robison, R.A., ed., p. 56-60.
- Harrison, J.E., 1972, Precambrian Belt Basin of northwest United

- States: its geometry, sedimentation, and copper occurrences: *Geol. Soc. Am. Bull.*, v. 83, p. 1215-1240.
- Harrison, J.E., Griggs, A.B., and J.D. Wells, 1981, Generalized geologic map of the Wallace 1 x 2 quadrangle, Montana and Idaho: U.S.G.S. Misc. Field Studies map MF-1854-A.
- Harrison, J.E., Griggs, A.B., and Wells, J.D., 1986, Geologic and structure maps of the Wallace 1 x 2 Quadrangle, Montana and Idaho: Montana Bureau of Mines and Geology, Montana atlas 4-A.
- Hietanen, A., 1968, Belt series in the region around Snow Peak and Mallard Peak, Idaho: U.S.G.S. Prof. Paper 344-E, 34 p.
- Hietanen, A., 1984, Geology along the northwest border zone of the Idaho batholith, northern Idaho: U.S. Geological Survey Bulletin 1608, 17 p.
- Hood, A., Gutjahr, C.C.M., and R.L. Heacock, 1975, Organic metamorphism and the generation of petroleum: *AAPG Bulletin*, v. 59, p. 986-996.
- Hunter, R., 1984, A structural and stratigraphic analysis of Belt Supergroup rocks, northern edge of the Sapphire allochthon, western Montana, unpublished senior thesis, Univ. of Montana, 60 p.
- Hyndman, D.W., 1985, Petrology of igneous and metamorphic rocks: McGraw-Hill Co., New York, 786 p.
- Hyndman, D.W., Alt, D., and J.W. Sears, 1987, Metamorphic and tectonic evolution of western Montana and northern Idaho: manuscript, 60 p.
- Jacobson, D., 1981, Rocks of the Ravalli Group mapped within the National Bison Range, Moise, Montana: unpublished senior thesis, University of Montana.
- Jennings, S., and G.R. Thompson, 1986, Diagenesis of Plio-Pleistocene sediments of the Colorado River delta, southern California: *J. Sed. Pet.*, v. 56, p. 89-98.
- Kauffman, M.E., 1963, Geology of the Garnet-Bearmouth area, western Montana: Montana Bureau of Mines and Geology, Mem. 39, 40 p.
- Lang, H. M., and J.M. Rice, 1985, Metamorphism of pelitic rocks in the Snow Peak area, northern Idaho: sequence of events and regional implications: *Geol. Soc. Am. Bull.*, v. 96, p. 731-736.
- Mackie, T.L., 1986, Tectonic influences on the petrology, stratigraphy and structures of the upper Cretaceous Golden Spike Formation, central-western Montana: master's thesis, Washington State Univ., 132 p.

- Mauk, J.L., 1983, Stratigraphy and sedimentation of the Proterozoic Burke and Revett Formations, Flathead Reservation, western Montana: master's thesis, Univ. of Montana, 91 p.
- Maxwell, J., 1965, Structure map and cross sections, southeast Drummond area: Billings Geol. Soc. Annual Field Conf., map.
- McDowell, F.W., 1971, K-Ar ages of igneous rocks from the western United States: *Isochron/West*, no. 2, p. 1-16.
- McDowell, S.D., and W.A. Elders, 1980, Authogenic layer silicate minerals in Borehold Elmore I, Salton Sea geothermal field, California, USA: *Contrib. Min. Pet.*, v. 74, p. 293-310.
- McMechan, M.E., and R.A. Price, 1982, Superimposed low-grade metamorphism in the Mount Fisher area, southeastern British Columbia-implications for the East Kootenay orogeny: *Can J. Earth Sci.*, v. 19, p. 476-489.
- Minnich, G.W., 1984, The timing of metamorphism relative to the rock fabrics in the Silver Hill Formation near the Garnet stock: unpublished senior thesis, Univ. of Montana, 11 p.
- Mitra, G., and W.A. Yonkee, 1984, Solution cleavage and its relationship to major structures in the Idaho-Utah-Wyoming thrust belt: *Geology*, v. 12, p. 354-358.
- Mitra, G., and W.A. Yonkee, 1985, Relationship of spaced cleavage to folds and thrusts in the Idaho-Utah-Wyoming thrust belt: *J. Struct. Geo.*, v. 7, p. 361-373.
- Montgomery, J.K., 1958, Geology of the Nimrod area, Granite County, Montana: master's thesis, Univ. of Montana, 61 p.
- Mutch, T.S., 1961, Geologic map of the northwest flank of the Flint Creek Range, western Montana: Montana Bureau of Mines and Geology, Spec. Publ. 21, Geologic Map 5.
- Nelson, W.H., and J.P. Dobel, 1961, Geology of the Bonner Quadrangle, Montana, U.S.G.S. Bull. 1111-F, Pl. 35.
- Nold, J.L., 1974, Geology of the northeastern border zone of the Idaho batholith, Montana and Idaho: *Northwest Geology*, v. 3, p. 47-54.
- Norwick, S.A., 1972, The regional Precambrian metamorphic facies of the Prichard Formation of western Montana and northern Idaho: Ph.D. Dissertation, University of Montana, 129 p.
- Ort, K.M., in progress, Ductile strain and thrust fault development in

- the Jocko Mountains, west-central Montana: master's thesis, Univ. of Montana.
- Oxburgh, E.R., and D.L. Turcotte, 1974, Thermal gradients and regional metamorphism in overthrust terrains with special reference to the eastern Alps: *Schweiz. Miner. Petrogr. Mitt.*, v. 54, p. 641-662.
- Ramsay, J.G., and M.I. Huber, 1983, *The techniques of modern structural geology, volume 1: strain analysis*: Academic Press, inc., 307 p.
- Reks, I.J., and D.R. Gray, 1983, Strain patterns and shortening in a folded thrust sheet: an example from the southern Appalachians: *Tectonophysics*, v. 93, p. 99-128.
- Richardson, S.W., and P.C. England, 1979, Metamorphic consequences of crustal eclogite production in overthrust orogenic zones: *Earth. planet. Sci. Lett.*, v. 42, p. 183-190.
- Rowe, D.W., 1984, Structural analysis of the Lolo Creek Fault area, northern edge of the Bitterroot dome, west-central Montana: unpublished senior thesis, Univ. of Montana, 45 p .
- Royden, L., and K.V. Hodges, 1984, A technique for analyzing the thermal and uplift histories of eroding orogenic belts: a Scandanavian example: *J. Geoph. Res.*, v. 89, p. 7091-7106.
- Ruppel, E.T., Wallace, C.E., Schmidt, R.G., and D.A., Lopez, 1981, Preliminary interpretation of the thrust belt in southwest and west-central Montana and east central Idaho: *Montana Geol. Soc. Field Conf. Southwest Montana*, p. 139-159.
- Sears, J.W., 1985, Implications of small-scale structures under the Sapphire plate, west-central Montana: *Geol. Soc. Am. Abstracts with Programs*, v. 17, p. 264.
- Sears, J.W., 1986, A two thrust-slab model for the central Montana-Idaho overthrust belt, and its relationship to the Rocky Mountain Foreland: *Geol. Soc. Am. Abstracts with Programs*, v. 18, p. 412.
- Sears, J.W., Ort, K.M., Thomas, M.B., and J.H. Griffen, 1986, Post-early Eocene clockwise fault block rotations along the Lewis and Clark line, west-central Montana: *Geol. Soc. Am. Abstracts with Programs*, v. 18, p. 412
- Sears, J.W. and C.P. Weiss, 1986, Deep thermal structure of the cordilleran thrust system, western Montana: *Geol. Soc. Am. Abstracts with Programs*, v. 18, p. 743.
- Selkman, S.O., 1983, Stress and displacement distributions around pyrite grains, *J. of Struc. Geo.*, v. 5, p. 47-52.

- Shelton, J.W., 1962, Shale compaction in a section of Cretaceous Dakota Sandstone, northwestern North Dakota: *J. Sed. Petr.*, v. 32, p. 873-877.
- Siddans, A.W.B., Henry, B., Kligfield, R., Lowrie, W., Hart, A., and M.N. Percevault, 1984, Finite strain patterns and their significance in Permian rocks of the Alpes Maritimes (France): *J. Struc. Geo.*, v. 6, p. 339-368.
- Simpson, C., 1983, Displacement and strain patterns from naturally occurring shear zone terminations: *J. Struc. Geo.*, v. 5, p. 497-506.
- Stuart, C.J., 1966, Metamorphism in the Flint Creek Range, Montana: master's thesis, Univ. of Montana, 103 p.
- Thomas, M.B., 1987, Structural geology along part of the Blackfoot fault system near Potomac, Missoula County, Montana: master's thesis, University of Montana.
- Thompson, A.B., and P.C. England, 1984, Pressure-temperature-time paths of regional metamorphism II. Their inferences and interpretation using mineral assemblages in metamorphic rocks: *J. of Petr.*, v. 25, p. 929-955.
- Toth, M.I., 1987, Petrology and origin of the Bitterroot lobe of the Idaho batholith: U.S.G.S. Prof. Paper 1436, p. 9-36.
- Turner, F.J., 1981, Metamorphic petrology: mineralogical, field, and tectonic aspects, McGraw-Hill Co., New York, 524 p.
- Wallace, C.E., Schmidt, R.G., Lidke, D.E., Waters, M.R., Elliott, J.E., French, A.B., Whipple, J.W., Zarske, S.E., Blaskowski, M.J., Heise, B.A., Yoeman, R.A., O'Neill, J.M., Lopez, D.A., Robinson, G.D., and M.R. Klepper, 1987, Preliminary map of the Butte 1 x 2 quadrangle, western Montana: U.S.G.S., open file report 86-292, map and text, 16 p.
- Watson, I.A., 1984, Structure of the Rattlesnake area, west-central Montana: master's thesis, Univ. of Montana, 55 p.
- Winkler, H.G.F., 1982, Petrogenesis of metamorphic rocks: Springer-Verlag, New York, 348 p.
- Wood, D.S., 1973, Patterns and magnitudes of natural strain in rocks: *Phil. Trans. R. Soc. Lond.*, v. A274, p. 373-382.
- Woodward, N.B., Gray, P.R., and D.B. Spears, 1986, Including strain data in balanced cross-sections: *J. of Struc. Geo.*, v. 8, p. 313-324.

APPENDIX A

STRATIGRAPHY AND STRUCTURAL BEHAVIOR OF UNITS

SYMBOL	THICKNESS	FORMATIONS	SOURCE	LITHOLOGY/STRUCTURAL BEHAVIOR
K <sub>gs</sub>	1830 m	upper Cretaceous Golden Spike Formation	1	Conglomerates, shales, and volcaniclastics contain spaced cleavage and small-scale folds and thrusts.
K <sub>s</sub>	3577 m	Cretaceous Carter Creek, Jens, Coberly, Blackleaf, and Kootenai Formations	2	Interlayered sandstones, shales, limestones, and conglomerates deformed with spaced cleavage, pencil cleavage, tension gashes, and small-scale folds and thrusts.
J	146 m	Jurassic Ellis Group	2	Siltstones and sandstones con- tain spaced cleavage and deformed by folding and thrusting.
P	128 m	Pennsylvanian Quadrant and Amsden Formations	2	Orthoquartzite and siltstone shortened with buckle folds.
Mm	701 m	Mississippian Madison Formation	2	Limestone with chert formed small-scale folds.
D	330 m	Devonian Jefferson and Maywood Formations	2	Dolomitic limestone and calcareous sandstone shortened with spaced cleavage.
Ch	436 m	Cambrian Red Lion and Hasmark Formations	2	Limestone and dolomite contained breccia zones and spaced cleavage.
cs	130 m	Cambrian Silver Hill Formation	3	Shale and limestone shortened with spaced cleavage, pencil cleavage, breccia zones.

SYMBOL	THICKNESS	FORMATIONS	SOURCE	LITHOLOGY/STRUCTURAL BEHAVIOR
<b>Empi</b>	360 m	Proterozoic Pilcher Formation	4	Quartzite deformed with breccia zones and buckle folds and thrusts.
<b>Emgr</b>	1170 m	Proterozoic Garnet Range Formation	4	Mica-rich quartzite contains spaced cleavage and slaty cleavage, breccia zones, and small-scale faults, folds, and kink folds.
<b>Emmc</b>	1200 m	Proterozoic MacNamara Formation	4	Siltites, argillites, and quartzites deformed with spaced cleavage, slaty cleavage, slickensides, and tension gashes.
<b>Embo</b>	400 m	Proterozoic Bonner Formation	4	Feldspathic quartzite shortened by buckle folding and contains spaced and slaty cleavage.
<b>Emms</b>	1600 m	Proterozoic Mount Schields Formation	4	Siltites, argillites, and quartzites sheared locally producing a stretching lineation, phyllitic and slaty cleavage and also contains spaced cleavage.
<b>EmsH</b>	460 m	Proterozoic Shepherd Formation	4	Dolomitic siltite and argillite commonly sheared, producing stretching lineations, phyllitic and slaty cleavage.
<b>Emsn</b>	1100 m	Proterozoic Snowslip Formation	4	Argillites, siltites, and quartzites contained spaced and occasional slaty cleavage.
<b>Emw Emh</b>	2740 m	Proterozoic Wallace- Helena Formation	5	Limestone, limey argillite, and limey siltite commonly sheared, producing stretching lineations, phyllitic and slaty cleavage.

SYMBOL	THICKNESS	FORMATIONS	SOURCE	LITHOLOGY/STRUCTURAL BEHAVIOR
Emsr	610 m	Proterozoic St. Regis Formation	6	Siltite, argillite, and quartzite sheared producing phyllitic and slaty cleavage.
Emr	900 m	Proterozoic Revett Formation	7	Quartzite deformed by spaced cleavage.
Emb	1000 m	Proterozoic Burke Formation	7	Siltite, argillite, and quartzite sheared producing phyllitic and slaty cleavage.
Empu	945 m	Proterozoic upper Prichard Formation	8	Siltite, argillite, and quartzite commonly sheared, producing a stretching lineation, phyllitic and slaty cleavage.
Empl	>6000 m	Proterozoic lower Prichard Formation	8	Quartzites contained spaced cleavage, while less common argillite layers contained phyllitic and slaty cleavage.
Tv	not known	Tertiary Volcanics		Undeformed rhyolites and volcanoclastics.
Kg	not known	Cretaceous Intrusions		Granite, deformed locally at contact zones, contained a spaced cleavage.
$\sigma P$	not known	Proterozoic Sills		Diabase sills, largely undeformed, locally sheared, producing a mylonitic fabric, mineral lineations, phyllitic and slaty cleavage.

#### SOURCES

1. Gwinn and Mutch, 1965
2. Mutch, 1961
3. Thomas, 1987
4. Watson, 1984
5. Desormier, 1975
6. Campbell, 1960
7. Mauk, 1983
8. Cressman, 1985

APPENDIX B

WESTERN PLATE MINERAL ASSEMBLAGES

SOURCE	M1 ASSEMBLAGE	M2 ASSEMBLAGE
Hietanen, 1984	sillimanite-kyanite- muscovite-quartz	-
Nold, 1974 and Chase, 1973	sillimanite-orthoclase- muscovite-biotite-quartz	-
Childs, 1982	sillimanite-kyanite- staurolite-biotite- muscovite-quartz	-
Carey and Rice, 1985	kyanite-sillimanite	andalusite
Carey and Rice, 1985	kyanite-sillimanite- staurolite-garnet-biotite	cordierite
Lang and Rice, 1985	kyanite-garnet-biotite- muscovite-quartz-plagioclase	sericite on staurolite
Chase and Johnson, 1975	kyanite-staurolite	cordierite
Hyndman et al., 1987	-	muscovite-biotite

## APPENDIX C

## EASTERN PLATE MINERAL ASSEMBLAGES

Precambrian metamorphism assemblages

SAMPLE	FORMATION	ASSEMBLAGE
5	Lower Prichard	biotite-muscovite-plagioclase-quartz
6	Lower Prichard	biotite-muscovite-plagioclase-quartz
9	Upper Prichard	biotite-muscovite-plagioclase-quartz
10	Upper Prichard	biotite-muscovite-plagioclase-quartz
11	Burke	biotite-muscovite-plagioclase-quartz
12	Upper Prichard	biotite-muscovite-plagioclase-quartz
14	Upper Prichard	biotite-muscovite-plagioclase-quartz
15	Lower Prichard	biotite-muscovite-plagioclase-quartz
16	Lower Prichard	biotite-muscovite-quartz
17	Lower Prichard	biotite-garnet-muscovite-plagioclase-quartz
18	Lower Prichard	biotite-muscovite-plagioclase-quartz
19	Lower Prichard	biotite-muscovite-plagioclase-quartz
20	Lower Prichard	biotite-muscovite-plagioclase-quartz
21	Lower Prichard	biotite-muscovite-plagioclase-quartz
22	Lower Prichard	biotite-muscovite-plagioclase-quartz
23	Lower Prichard	biotite-garnet-hornblende-plagioclase-muscovite-quartz
24	Lower Prichard	biotite-muscovite-quartz
25	Wallace	muscovite-calcite-plagioclase-dolomite-quartz
30	St. Regis	muscovite-plagioclase-quartz
31	Upper Prichard	muscovite-quartz
36	Burke	biotite-muscovite-quartz
43	Revett	muscovite-plagioclase-quartz
45	Burke	biotite-muscovite-plagioclase-quartz
46	Burke	biotite-muscovite-quartz
48	Snowslip	muscovite-quartz
49	St. Regis	biotite-muscovite-plagioclase-quartz
52	Burke	biotite-muscovite-quartz
53	Upper Prichard	biotite-muscovite-plagioclase-quartz
56	Upper Prichard	biotite-muscovite-quartz
57	Upper Prichard	biotite-muscovite-quartz
58	Upper Prichard	biotite-garnet-muscovite-quartz
59	Upper Prichard	muscovite-plagioclase-quartz
60	Upper Prichard	biotite-muscovite-quartz
62	Upper Prichard	biotite-muscovite-quartz
63	Lower Prichard	biotite-muscovite-quartz
64	Lower Prichard	biotite-muscovite-quartz
65	Lower Prichard	biotite-muscovite-quartz
66	Lower Prichard	biotite-muscovite-quartz

SAMPLE	FORMATION	ASSEMBLAGE
67	Lower Prichard	biotite-muscovite-quartz
70	Lower Prichard	biotite-garnet-hornblende-muscovite-plagioclase-quartz
71	Lower Prichard	biotite-garnet-hornblende-muscovite-plagioclase-quartz
72	Lower Prichard	biotite-garnet-hornblende-muscovite-plagioclase-quartz
75	Lower Prichard	biotite-muscovite-quartz
76	Burke	biotite-muscovite-quartz
79	Snowslip	muscovite-quartz
80	Snowslip	muscovite-quartz
83	Burke	biotite-muscovite-plagioclase-quartz
84	Burke	biotite-muscovite-plagioclase-quartz
88	Wallace	calcite-dolomite-muscovite-plagioclase-quartz
90	MacNamara	muscovite-calcite-plagioclase-quartz
93	Bonner	muscovite-plagioclase-quartz
95	Garnet Range	muscovite-plagioclase-quartz
96	Garnet Range	muscovite-plagioclase-quartz
97	Garnet Range	muscovite-plagioclase-quartz
98	MacNamara	muscovite-plagioclase-quartz
99	MacNamara	muscovite-plagioclase-quartz
100	Bonner	muscovite-plagioclase-quartz
101	Bonner	muscovite-plagioclase-quartz
102	MacNamara	chlorite-muscovite-plagioclase-quartz
103	MacNamara	muscovite-plagioclase-quartz
105	Garnet Range	muscovite-plagioclase-quartz
111	Bonner	muscovite-quartz
112	MacNamara	chlorite-muscovite-quartz
113	MacNamara	muscovite-plagioclase-quartz
114	MacNamara	muscovite-plagioclase-quartz
115	MacNamara	muscovite-plagioclase-quartz
116	Bonner	muscovite-plagioclase-quartz
117	Mount Shields	chlorite-muscovite-plagioclase-quartz
123	Lower Prichard	biotite-muscovite-calcite-plagioclase-quartz
124	Lower Prichard	biotite-garnet-hornblende-muscovite-quartz
125	Lower Prichard	biotite-garnet-muscovite-quartz
126	Lower Prichard	biotite-muscovite-quartz

Cretaceous metamorphism assemblages

SAMPLE	FORMATION	ASSEMBLAGE
5	Lower Prichard	biotite-chlorite-muscovite-plagioclase-quartz
6	Lower Prichard	biotite-chlorite-muscovite-plagioclase-quartz
7	Lower Prichard	biotite-muscovite-quartz
8	Lower Prichard	biotite-muscovite-quartz
9	Upper Prichard	chlorite-muscovite-quartz
10	Upper Prichard	chlorite-muscovite-pyrite-quartz
12	Upper Prichard	chlorite-muscovite-quartz
13	Upper Prichard	muscovite-quartz
15	Lower Prichard	biotite-chlorite-muscovite-plagioclase-quartz
16	Lower Prichard	biotite-chlorite-muscovite-plagioclase-quartz
17	Lower Prichard	biotite-chlorite-muscovite-plagioclase-quartz
21	Lower Prichard	biotite-chlorite-muscovite-quartz
23	Lower Prichard	chlorite-muscovite-quartz
25	Wallace	calcite-dolomite-muscovite-plagioclase-quartz
26	Snowslip	chlorite-calcite-dolomite-muscovite-quartz
27	Snowslip	chlorite-calcite-muscovite-quartz
28	Snowslip	calcite-muscovite-quartz
29	Wallace	calcite-dolomite-muscovite-plagioclase-quartz
32	Upper Prichard	chlorite-muscovite-pyrite-quartz
33	Upper Prichard	muscovite-pyrite-quartz
34	Upper Prichard	muscovite-pyrite-quartz
35	Burke	chlorite-muscovite-pyrite-quartz
36	Burke	chlorite-muscovite-quartz
37	Lower Prichard	chlorite-muscovite-quartz
38	Prec. sill	chlorite-calcite-quartz
39	Prec. sill	chlorite-calcite-plagioclase-quartz
40	Lower Prichard	muscovite-plagioclase-quartz
43	Revett	muscovite-plagioclase-quartz
44	Revett	muscovite-plagioclase-quartz
45	Burke	chlorite-muscovite-pyrite-plagioclase-quartz
46	Burke	chlorite-muscovite-plagioclase-quartz
47	Burke	chlorite-muscovite-quartz
48	Snowslip	chlorite-muscovite-quartz
49	St. Regis	chlorite-muscovite-quartz
51	Upper Prichard	chlorite-muscovite-pyrite-plagioclase-quartz
54	Upper Prichard	chlorite-muscovite-pyrite-plagioclase-quartz

SAMPLE	FORMATION	ASSEMBLAGE
55	Upper Prichard	chlorite-muscovite-pyrite-quartz
56	Upper Prichard	chlorite-muscovite-quartz
58	Upper Prichard	chlorite-muscovite-quartz
61	Upper Prichard	chlorite-muscovite-quartz
62	Upper Prichard	chlorite-muscovite-quartz
63	Lower Prichard	chlorite-muscovite-quartz
65	Lower Prichard	chlorite-muscovite-plagioclase-quartz
66	Lower Prichard	chlorite-muscovite-plagioclase-quartz
68	Lower Prichard	biotite-muscovite-quartz
69	Lower Prichard	biotite-muscovite-quartz
78	St. Regis	chlorite-muscovite-quartz
79	Snowslip	muscovite-quartz
80	Snowslip	muscovite-quartz
81	Wallace	chlorite-muscovite-plagioclase-quartz
82	Wallace	muscovite-quartz
83	Burke	chlorite-muscovite-plagioclase-quartz
84	Burke	chlorite-muscovite-plagioclase- pyrite-quartz
85	Wallace	chlorite-muscovite-quartz
86	Wallace	muscovite-quartz
87	Wallace	muscovite-calcite-quartz
88	Wallace	dolomite-calcite-plagioclase- muscovite-quartz
92	Wallace	calcite-muscovite-quartz
94	Garnet Range	muscovite-plagioclase-quartz
100	Bonner	muscovite-plagioclase-quartz
103	MacNamara	muscovite-plagioclase-quartz
104	Garnet Range	muscovite-plagioclase-quartz
106	Wallace	calcite-dolomite-muscovite- plagioclase-pyrite-quartz
118	Prec. sill	chlorite-plagioclase-muscovite-quartz
119	Mount Shields	chlorite-calcite-dolomite-pyrite- plagioclase-muscovite-quartz
120	Mount Shields	chlorite-muscovite-plagioclase-quartz
121	Mount Shields	chlorite-dolomite-calcite- plagioclase-muscovite-quartz
122	Mount Shields	calcite-dolomite-plagioclase- muscovite-quartz
127	Lower Prichard	biotite-muscovite-quartz
129	Mount Shields	muscovite-quartz
130	Prec. sill	chlorite-actinolite-epidote-calcite- plagioclase-quartz
131	Prec. sill	chlorite-actinolite-epidote-calcite- plagioclase-quartz

## APPENDIX D

### STRAIN MEASUREMENTS

#### Shear Strain

For deformed sandstone dikes, I measured the angle "psi" for each sandstone dike, where psi is the angle between the present deformed sandstone dike and its original state, perpendicular to bedding. From the angle psi, I obtained the shear strain from the following equation:

$$\text{shear strain} = \tan (\text{psi})$$

Sample 54 is from the upper Prichard Formation, while sample 129 is from the Mount Shields Formation.

SAMPLE	PSI (IN DEGREES)	SHEAR STRAIN
54	78	4.7
	69	2.6
	65	2.1
	69	2.6
	average =	3.5
129	38	0.78
	48	1.1
	34	0.67
	46	1.0
	average =	0.90

#### Pyrite Pressure Shadows

To measure the strain in pyrite pressure shadows, I determined the maximum elongation (X) from the equation:

$$X = (1 + \text{principle elongation}), \text{ where}$$

$$\text{principle elongation} = \frac{\text{fiber length}}{\text{pyrite radius}}$$

All determinations of principle elongation came from thin-sections of samples cut perpendicular to cleavage. In this appendix I also provided measurements from orthogonal cuts. All measurements are in x/100 mm. Sample 119 comes from the Mount Shields Formation, while all others are from the upper Prichard Formation.

SAMPLE	FIBER LENGTH	PYRITE RADIUS	MAXIMUM ELONGATION
10	22	5	5.4
	15	7	3.1
	20	8	3.5
	8	5	2.6
			average = 3.6
32	10	7	2.4
	8	3	3.7
	12	4	4.0
	9	4	3.2
	8	4	3.0
	7	3	3.3
			average = 3.3
33	20	5	5.0
	24	6	5.0
	40	5	9.0
	20	3	7.7
	16	3	6.3
	30	4	8.5
	20	4	6.0
	25	4	7.2
	33	6	6.5
	19	5	4.8
	16	2	9.0
	11	3	4.7
			average = 6.7
34	22	6	4.7
	29	5	6.8
	17	3	6.7
	28	4	8.0
	20	3	7.7
	32	7	5.6
	17	3	6.7
	30	4	8.5
	15	3	6.0
	29	5	6.8
	36	4	10.0
	18	4	5.5
	23	4	6.8
	31	5	7.2
	26	5	6.2
27	4	7.8	

SAMPLE	FIBER LENGTH	PYRITE RADIUS	MAXIMUM ELONGATION
34	29	4	8.2
	19	3	7.3
	30	4	8.5
	25	5	6.0
			average = 7.0
51	30	4	8.5
	14	3	5.7
	19	4	5.8
	27	5	6.4
	17	4	5.2
	20	3	7.7
	12	4	4.0
	21	4	6.2
	15	3	6.0
	17	5	4.4
	7	2	4.5
			average = 6.0
54	22	4	6.5
	26	5	6.2
	16	4	5.0
	14	3	5.6
	26	6	5.3
	24	4	7.0
	14	6	3.3
	21	4	6.2
			average = 6.6
55	10	3	4.3
	6	4	2.5
	7	5	2.4
	9	5	2.8
			average = 3.0
119	11	6	2.8
	8	4	3.0
	4	2	3.0
	8	3	3.7
	20	3	4.3
	21	7	4.0
			average = 3.5

Measurements from orthogonal cuts

SAMPLE	FIBER LENGTH	PYRITE RADIUS
10	8	6
	14	4
	17	6
	28	6
	10	5
	15	7
	25	5
	23	6
	11	4
	28	4
	27	6
	8	3
	20	6
	9	7
	32	21
11		3
19		4
15		3
14		4
15		3
17		3
16		4
29		4
27		6
24		4
13		3
32		5
29		6
12		3
33	40	4
	31	5
	20	4
	17	5
	27	5
	16	5
	12	4
	30	5
	19	4
	11	3
	25	4
	9	3
	31	4
	16	3
	33	6

	27	5
34	38	6
	28	5
	25	4
	34	5
	35	5
	30	5
	32	4
	44	7
	27	5
	28	4
	33	6
51	42	9
	30	4
	13	4
	12	3
	24	7
	32	6
	27	8
	33	5
	29	4
54	12	4
	16	3
	8	3
	25	6
	17	4
	13	5
	13	6
	12	6
	16	8
55	6	3
	7	4
	10	3
119	13	3
	8	3
	8	4
	15	4
	11	3
	12	8